INVESTIGATION OF NANOSCALE DRUG PARTICLES AND THEIR EFFECT ON THE FLUID DYNAMIC PROPERTIES OF THE BLOOD

By

Jason L. Slats, B.S.

A project report submitted in partial fulfillment of

the requirements for the degree of

Master of Science

in

Mechanical Engineering

University of Alaska Fairbanks

May 2020

APPROVED:

Debendra Das, Committee Chair
Lei Zhang, Committee Co-Chair
Debasmita Misra, Committee Member
Rorik Peterson, Chair
Department of Mechanical Engineering

Abstract

Research has shown that gold nanoparticles increase the efficiency of radiation treatments of cancer by up to 25%. This means patients can be exposed to lower doses of radiation that does more concentrated damage to cancerous cells and less damage to healthy surrounding tissue. Before these nanoparticles can be introduced to the human body, the behavior of these particles in the blood stream must be understood. A model of gold nanoparticle flow through the aortic arch was developed in the present investigation for predicting behavior of these particles in the human body.

A set of initial modeling parameters was developed out of existing data pertaining to blood flow rates and viscosities of a blood-mimicking fluid across a temperature range of 30-40 degrees Celsius. The aorta wall was modeled as a no-slip solid surface. Computational fluid dynamic models using ANSYS Fluent across this temperature range have generated general velocity distributions of blood flow through the aortic arch and identifies several areas of possible recirculation. The current state of the model provides preliminary results, which are valuable in generating an accurate model of gold nanoparticles flowing through the aortic arch.

INVESTIGATION OF NANOSCALE DRUG PARTICLES AND THEIR EFFECT ON THE FLUID DYNAMIC PROPERTIES OF THE BLOOD

By

Jason L. Slats

APPROVED: Dr. Debendra Das
Advisory Committee Co-Chair

Dr. Lei Zhang
Advisory Committee Co-Chair

Dr. Debasmita Misra
Advisory Committee Member

Dr. Rorik Peterson
Chair, Department of Mechanical Engineering

Date: April 6, 2019

Contents

List of Figures

Chapter 1: Introduction

1.1 Nanotechnology in Treating Cancer

Cancer has directly or indirectly affected numerous living beings, including many Alaskans. Research from the Alaska Native Tribal Health Consortium shows that cancer is the leading cause of death among Alaska Native populations (at a rate 10-20 percent higher than the national average). Advances in technology offer the potential for cancer and disease treatment. Nanotechnology is becoming increasingly widespread in today's industries including the field of biomedicine. Research has shown that gold nanoparticles introduced to cancerous tissue can improve effectiveness of killing those cancer cells with radiation by up to 25% [1]. During the course of their research, Antosh et al [1] determined a stable material with a high atomic number would be ideal for this application. They applied gold nanoparticles to samples of cancerous lung tissue in vitro and irradiated them with an x-ray machine.

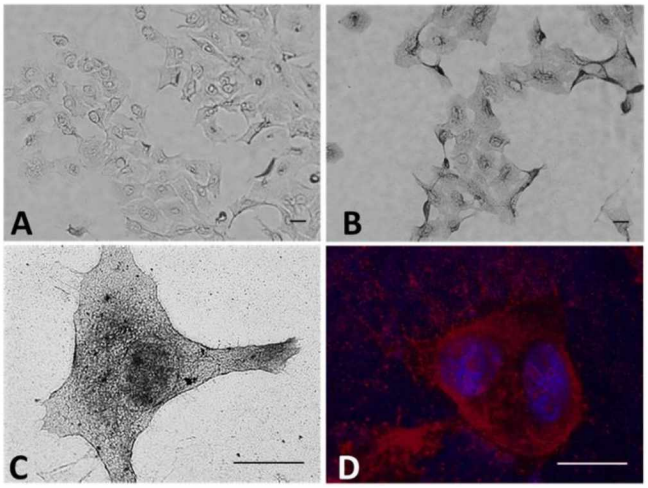

Figure 1: Samples of cancerous lung tissue with gold nanoparticles

Figure 1 shows samples of cancerous lung tissue with gold nanoparticles under a microscope. Sample A shows gold nanoparticles alone, while samples B-D utilize nanoparticles that were functionalized to bond with a protein that bounces off of healthy tissue and attaches itself to diseased tissue [1]. The enhanced destruction of the cancer cells comes from the Auger Effect, in which energy from the x-ray causes an electron in the outer shell of the gold nanoparticle to

move to a higher energy shell. This causes another electron from an outer shell to be ejected into the surrounding cancerous tissue [1].

Applying nanotechnology in this way requires an understanding of how the human body will react to these nanoparticles. To help achieve this understanding, a computational fluid dynamic model of blood flow through the aortic arch could be developed using ANSYS Fluent. The modeling presented here represents how changes to viscosity of the fluid over a temperature range affect the velocity profiles of blood through the aortic arch. However, further investigation into how other thermophysical properties (density, thermal conductivity, and specific heat) are affected by the introduction of nanoparticles into the blood stream is required for a comprehensive study. In a cancer treatment application, gold nanoparticles may not flow through the heart. Flow through the aortic arch was chosen to model for its relatively simple geometry. When the model is refined, it can then be applied to more complex geometries where cancer tumors will be treated.

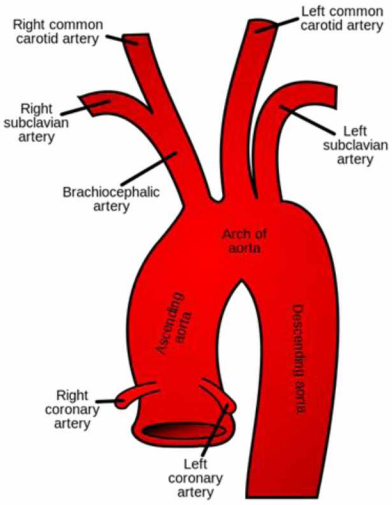

Figure 2: Diagram courtesy of University of California Department of Surgery https://surgery.ucsf.edu/conditions--procedures/aortic-arch-disease.aspx

The area being modeled starts above the coronary arteries, covers the entire arch including the three main artery branches on the top, and down the descending aorta to a point even with the starting point. The relatively simple geometry of this section will be used to refine the CFD model so that it can then be applied to more complex geometries.

1.2 Nanofluids Literature Review

Das, Choi, Yu and Pradeep [2] conducted significant research into the nature of and applications of nanofluids. Nanofluids are created by dispersing nanoscale solid particles into a fluid. The average size of these nanoparticles is generally below 100 nm. Extensive research has been conducted on how these types of fluids affect heat transfer. The intent of this research is to extract the most efficiency from a nanofluid with respect to thermal properties with the lowest concentration of nanoparticles in the fluid [2].

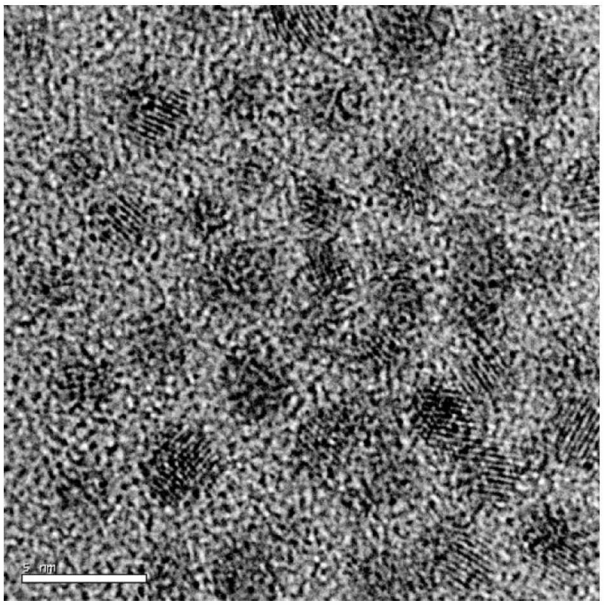

Figure 3:3 nm Gold Nanoparticles Synthesized by Chemical Reaction [2]

Cao and Wang [3] describe a variety of ways in which nanoparticles can be synthesized. There are several goals to consider when generating nanoparticles. The nanoparticles should all be of similar size and shape. The nanoparticles should also have the same chemical composition and structure and should not easily agglomerate. The particles should be easily separated if agglomeration does occur. Homogeneous nucleation is a method of nanoparticle synthesis in which generation occurs in a supersaturated solution. Nuclei are formed in the solution and growth occurs. Size and uniformity of the nanoparticles is determined by close control of the nucleus formation and subsequent growth. Metallic nanoparticles can be synthesized by reduction reactions of metallic compounds in a solution. Size of the nanoparticles using this method are controlled by the concentration of the solute and the introduction of a polymeric monolayer onto the growth surface to inhibit formation of nuclei. Hydrolysis is another method

of generating metal oxides in a solution. As the solution becomes oversaturated, the nucleation occurs [3].

There has been significant research into use of nanoparticles in the biomedical field. Sharifi, Shokrallahi, and Amiri [4] examined the properties of ferrite-based magnetic nanofluids. These types of fluids have possible uses in a form of cancer treatment called hyperthermia. Hyperthermia is simply the heating of cancerous regions using radio waves, microwaves, or lasers. Cancer cells are more susceptible to damage from heat than normal cells, so if these nanoparticles could be deployed to a localized area where cancerous cells are growing then hyperthermic treatments could be more effective [4].

Any deployment of nanoparticles for biomedical purposes will require functionalization of the nanoparticle with a protein or antibody. Rahme and Holmes [5] conducted a study on the bioconjugation of 60, 90, and 150 nm gold nanoparticles with an amino group of the apolipoprotein (ApoE) protein in water. This was accomplished using a functional oligomer based on ethylene glycol, thiol disulfide, and N-hydroxy succinimide [5].

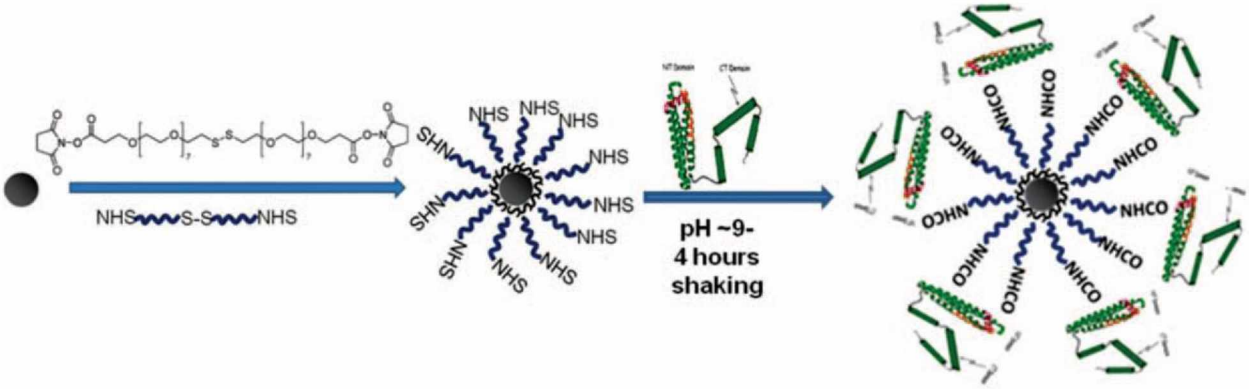

Figure 4: Formation of gold nanoparticles functionalized with ApoE Protein [5].

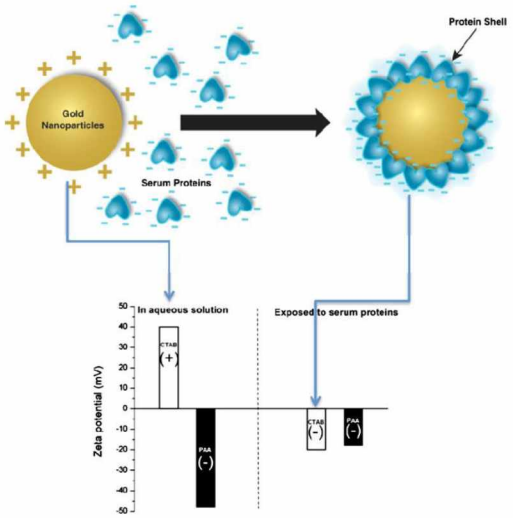

Figure 5: Gold nanoparticle with protein adsorption [6]

Understanding how these nanoparticles affect the human body is an important consideration before any biomedical trials involving living subjects can be implemented. Alkilany and Murphy [6] examined the nanotoxicity of gold. Gold is nonreactive and are already used in clinical settings as arthritis treatments, but gold nanoparticles are not currently used on human patients. Alkilany and Murphy [6] found that more research is required to understand gold nanoparticle toxicity. Studies on this topic have had conflicting results. No toxicity was found in mice for 3-5 nm gold nanoparticles and gold nanoparticles in the 50-100 nm range. Nanoparticle sizes in between these ranges were lethal to the mice and resulted in major internal organ damage. However, in vitro tests conducted with nanoparticles in the harmful 18-37 nm range were not found to be lethal. In all cases, gold nanoparticles were found in the liver and spleen after injection. Gold nanoparticles from the smaller size range were found in the brain and lungs as well [6]. Cedervall et al. [7] also showed that nanoparticles in the blood stream will adsorb to the surface of the nanoparticle changing its properties and behaviors as it becomes covered with the surrounding proteins.

Aggarwal et al.[8] explain that this adsorption of proteins to the nanoparticle happens as soon as the nanoparticle is in the biological system. A gold nanoparticle is a foreign object and subject to the body's biological response to its presence in the system. There is further study required to understand the protein binding and the effects this binding has on nanoparticle distribution,

biocompatibility of the nanoparticle, and the effect this bonding has on the biomedical value of the nanoparticle [8].

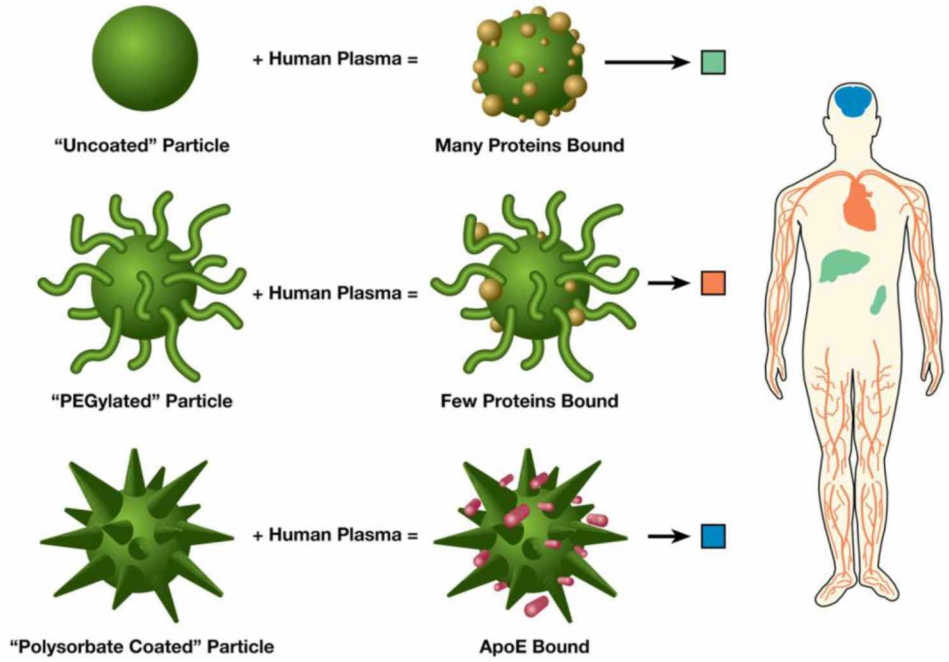

Figure 6: Bound proteins to several types of particles

1.3 Blood Viscosity

It is important to understand the properties of blood in order to understand how it flows. The Standard Handbook of Biomedical Engineering and Design [9] is an excellent reference for this information. Although blood is a non-Newtonian fluid, it is worth noting that in large arteries blood behaves as a Newtonian fluid.

$$\tau = \mu(-\frac{du}{dr}) \quad (1)$$

Equation 1 indicates shear stress (τ) is a linear function of blood viscosity (μ) where u is velocity and r is the distance from the aortic wall [9]. In smaller arteries the shear stress is not linear with the shear rate and acts as a non-Newtonian fluid. Equation 2 describes this relationship where K is a constant and n is greater than 0 [9].

$$\tau = K\left(-\frac{du}{dr}\right)^{n} \tag{2}$$

1.4 Governing Equations of the Fluid Dynamic Model

Since blood flow through large arteries can be characterized as Newtonian flow, the Navier-Stokes equation in cylindrical coordinates can be applied to describe the fluid flow. Equation 3 is the continuity equation and equations 4-6 are the momentum equations in the r, theta, and z directions [10].

$$\frac{1}{r}\frac{\partial}{\partial r}(rv_r) + \frac{1}{r}\frac{\partial}{\partial \theta}(v_\theta) + \frac{\partial}{\partial z}(v_z) = 0 \tag{3}$$

$$\frac{\partial v_r}{\partial t} + (\boldsymbol{V}\cdot\boldsymbol{\nabla})v_r - \frac{1}{r}v_\theta^2 = -\frac{1}{\rho}\frac{\partial p}{\partial r} + g_r + v(\nabla^2 v_r - \frac{v_r}{r^2} - \frac{2}{r^2}\frac{\partial v_\theta}{\partial \theta}) \tag{4}$$

$$\frac{\partial v_\theta}{\partial t} + (\boldsymbol{V}\cdot\boldsymbol{\nabla})v_\theta - \frac{v_r v_\theta}{r} = -\frac{1}{\rho}\frac{\partial p}{\partial \theta} + g_\theta + v(\nabla^2 v_\theta - \frac{v_\theta}{r^2} + \frac{2}{r^2}\frac{\partial v_r}{\partial \theta}) \tag{5}$$

$$\frac{\partial v_z}{\partial t} + (\boldsymbol{V}\cdot\boldsymbol{\nabla})v_z = -\frac{1}{\rho}\frac{\partial p}{\partial z} + g_z + v\nabla^2 v_z \tag{6}$$

Additional work using the Navier-Stokes equation to develop a one-dimensional model for arterial flow was developed by Formaggia, Lamponi, and Quarteroni [11]. They used a numerical method approach to average the Navier-Stokes equation across the different sections of the blood vessel. Similarly, Ghigo et al. [12] developed a 1-D non-Newtonian blood flow

model to be applied in smaller diameter blood vessels where a Newtonian assumption cannot be made. Equations 7 and 8 show the conservation of mass and momentum equations for the 1-D non-Newtonian system with an elastic boundary [12].

$$\frac{\partial A}{\partial t} + \frac{\partial Q}{\partial x} = 0 \tag{7}$$

Here A represents the cross-sectional area and Q is the axial flow rate.

$$\frac{\partial Q}{\partial t} + \frac{\partial}{\partial x}\left(\frac{Q^2}{A} + \frac{K}{2\rho}A^{\frac{3}{2}}\right) = \frac{2\pi R}{\rho}\tau_{rx} \tag{8}$$

In Equation 8, K is the rigidity of the arterial wall and τ_{rx} is the wall shear stress. Shear stress is directly linked to viscosity via Equation 1. This means that fluid viscosity plays a major role in studying the flow characteristics of a fluid. Extensive research has been conducted in determining how viscosity is affected by the addition of nanoparticles to a fluid.

1.5 Nanofluids Viscosity Correlations

In 1906, Einstein [13] developed a correlation for viscosity of a liquid "in which very many irregularly distributed small spheres are suspended." Equation 9 is his equation for determining the viscosity of this suspension based on the viscosity of the base fluid and the volume fraction (φ) of the particles in the fluid where k^* is the viscosity of the suspension and k is the viscosity of the base fluid.

$$k^* = k(1 - 2.5\,\varphi) \tag{9}$$

Following Einstein's lead was De Brujin [14] who modified Einstein's equation as shown in Equation 10. Here, μ_{eff} is the viscosity of the mixture and μ_{bf} is the viscosity of the base fluid while ϕ is the volume fraction of the particles in the base fluid.

$$\mu_{eff} = \mu_{bf}\left(\frac{1}{1 - 2.5\,\phi + 1.552\phi^2}\right) \tag{10}$$

Vladimir Vand [15] developed an equation that introduced a term to account for interaction between particles. He made the assumption that the particles will stay together for a short time and act as a single larger particle. The equation he came up with was only valid to the first term for this interaction. His equation is shown as Equation 11 [15].

$$\mu_{eff} = \mu_{bf}(1 - 2.5\,\phi + 7.349\phi^2 \ldots) \tag{11}$$

M. Mooney [16] built upon Einstein's equation to apply to a suspension with a finite concentration of particles. This expression includes a constant *K* called the self-crowding factor. Mooney's equation is shown below.

$$\mu_{eff} = \mu_{bf} \exp\left(\frac{2.5\phi}{1 - K\phi^2}\right) \tag{12}$$

In 1952, Brinkman [17] developed an equation that became widely used although it did not introduce any new terms. Brinkman's equation is shown below.

$$\mu_{eff} = \mu_{bf}\left(\frac{1}{(1 - \phi)^2}\right) \tag{13}$$

1.6 Properties of Blood Vessel Walls

The blood vessels themselves have important characteristics. The arterial wall is composed of 3 separate layers containing very different types of cells. The innermost layer, the intima, is made up of cells that keep the blood cells separated from the outer 2 layers of the vessel wall. The middle (and largest) layer is called the media. The media primarily consists of muscle cells with elastin and some collagen. Collagen is also found in the outermost layer of the vessel wall, the adventitia. Each layer is separated by a very thin elastic layer. Figure 7 shows clearly the

detailed layers of the wall [18]. For the purpose of creating a more realistic wall for a computational fluid dynamic model, each layer does not have to be individually created and assigned material properties. Several studies have been conducted that measure the mechanical properties of arteries and blood vessels.

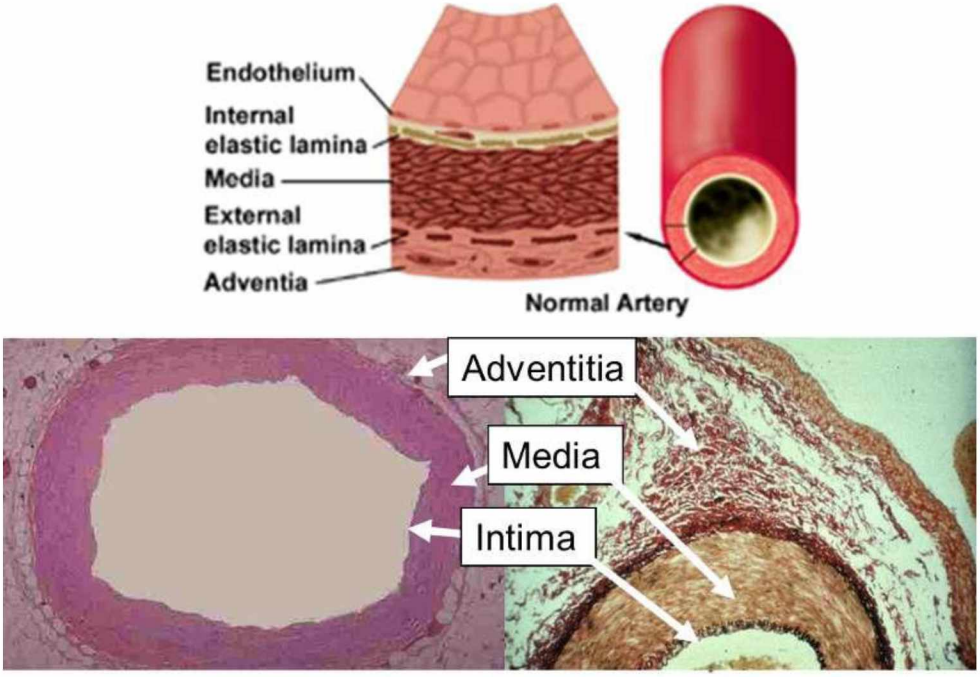

Figure 7: Blood Vessel Layers http://sphweb.bumc.bu.edu/otlt/MPH-Modules/PH/PH709_Heart/BloodVessel-structure.jpg

A team from the University of Madrid carried out stress testing on human coronary arteries. They were able to obtain samples from 5 brain-dead patients aged between 23 and 83. The patients did not suffer from any coronary disease. Each sample was at least 50 mm long, and uniaxial loading was applied at a rate of 0.03 mm/s until one of the layers mentioned above failed [19]. The following equations were used to define values for stress and stretch:

$$\lambda = \frac{l}{L} \tag{14}$$

$$a = \frac{A}{\lambda} \tag{15}$$

$$\sigma = \frac{P}{a} \tag{16}$$

Symbols for equations 14-16 are defined as follows:

λ is stretch, l is current length, and L is initial length. The value a is current cross-sectional area and A is initial cross-sectional area. σ is true stress and P is applied load. Results from the 5 samples were not similar enough to derive a single stretch-stress relationship across all samples. A general relationship is described by the stretch/stress plot in Figure 8.

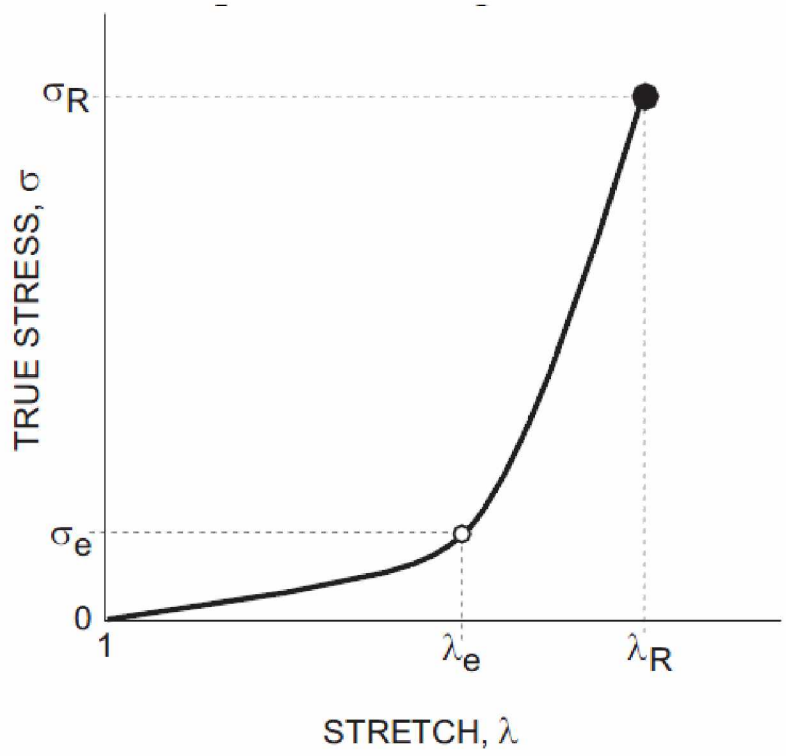

Figure 8: General Stress/Stretch relationship found in each sample after uniaxial testing

The plot can be broken down into 2 separate regimes. The first section of the plot defined from 1 to λ_e shows the region where the elastin in the artery wall dominates the response to the applied load [3]. The coordinate (λ_e, σ_e) was defined by the researchers as the midpoint where the first derivative of the plot in Figure 8 transitions from the first general elastic modulus to the second

much higher modulus. That second region is where the response to the applied load is dominated by the collagen layer of the artery wall [19].

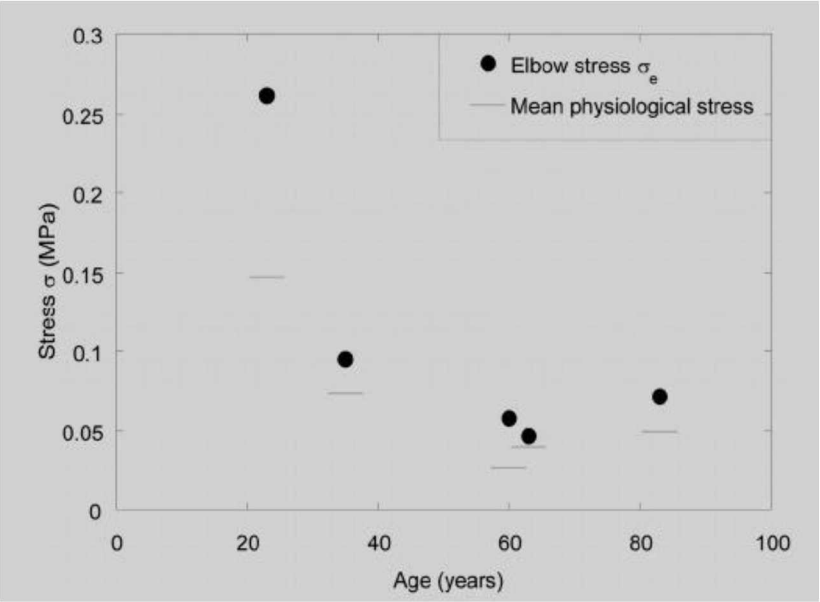

Figure 9: Elbow stresses across 5 samples [19]

Figure 9 represents the elbow stress point (it is the same as the transition point in Figure 8) of each of the 5 samples. Examining how the elbow stress fits into the overall stretch/stress plot in Figure 8, it is obvious that there is great deviation across each sample, and that a single usable value to apply to the mechanical properties of a model is not possible from this data set. Figure 9 shows that there is a five-fold increase in elbow stress as the age increases from 20 to 80.

Researchers from the Department of Mechanical Engineering and the Department of Biomedical Engineering in collaboration with researchers from the Division of Cardiothoracic Surgery at Washington University in St. Louis Missouri were able to perform both planar biaxial loading and strength testing on samples taken from 64 patients who were being treated for Marfan Syndrome. This is an excellent example of collaborative research between engineering and medicine faculty. According to the Marfan Foundation, Marfan Syndrome is a genetic disorder that may cause enlargement of the aorta and other connective tissue. Although the tissue

samples collected for this study may not represent healthy systems, the data collected during the study contributes to the understanding of the mechanical properties of arterial walls. It should be noted that the researchers performed a 3rd qualitative test to compare residual circumferential stress in the aorta between patients. However, since this was a qualitative test it will not contribute to the numerical values for mechanical properties needed for the computational fluid dynamics model and will not be discussed here.

Results of the uniform biaxial loading tests at Washington University were similar to what was found in the University of Madrid experiments. Figure 10 shows results from 2 of the 64 samples taken. The stiffer stress response (circles ●) is from a sample provided by a 65-year-old while the gentler sloped plot (triangles ▲) is from a 49-year-old patient [20].

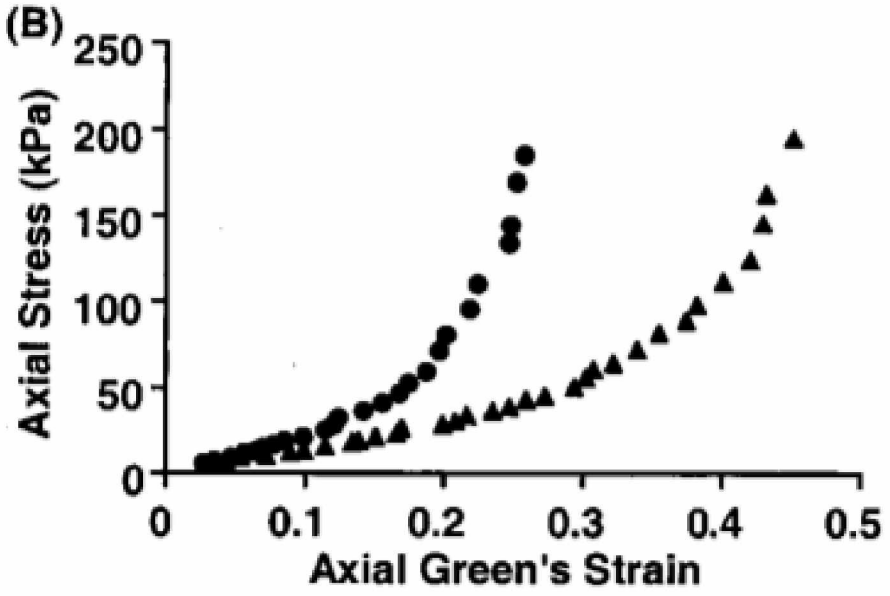

Figure 10: Stress/Strain plots provided by a 65 year old patient and a 49 year old patient [20]

Overall, results were too scattered to find a single average elastic modulus to apply to a mathematical model. However, Equation 17 calculates the failure stress based upon the strength tests conducted in the study [20].

$$\sigma_f[MPa] = 2.875 - 0.023(Age\ [Years]) \quad \textbf{(17)}$$

This equation can be used as a general estimate of what the failure stress will be. The limitation is this correlation only has an R^2 value of 0.44.

1.7 Summary of Different Chapters of this Report

Chapter 2 will provide viscosity data for blood. This data will be used as the input functions for viscosities of a blood-like fluid across a range of temperatures and gold nanoparticle concentrations.

Chapter 3 will present the ANSYS Fluent modeling conducted for this research.

Chapter 4 will provide the conclusion and recommendations for future work.

Appendix A provides all the results for the ANSYS Fluent modeling of blood flow through the aortic arch.

1.8 References

[1] Antosh, M. P., Wijesinghe, D. D., Shrestha, S., Lanou, R., Huang, Y. H., Hasselbacher, T., Fox, D., Neretti,N., Sun, S., Katenka, N., Cooper, L. N., Andreev, O. A., and Reshetnyak, Y. K., 2015, "Enhancement of radiation effect on cancer cells by gold-pHLIP," Proceedings of the National Academy of Sciences, 112(17), pp. 5372-5376.

[2] Das, Sarit K., Choi, S., Yu, W., and Pradeep, T. Nanofluids: Science and Technology. Lightning Source UK, 2015.

[3] Cao, Guozhong and Ying Wang. *Nanostructures and Nanomaterials:Synthesis, Properties, and Applications.* World Scientific, 2013.

[4] Sharifi, Ibrahim and Shokrollahi, Hooman. (2011). "Ferrite-based magnetic nanofluids used in hyperthermia applications." *Journal of Magnetism and Magnetic Materials*. 324. 903-905. 10.1016/j.jmmm.2011.10.017.

[5] Rahme, Kamil, and Justin D. Holmes. "Gold Nanoparticles: Synthesis, Characterization, and Bioconjugation." *Dekker Encyclopedia of Nanoscience and Nanotechnology, Third Edition,* 2015, pp. 1-11. *Crossref,* doi:10.1081/e-enn3-120053520.

[6] Alkilany, Alaaldin M, and Catherine J Murphy. "Toxicity and cellular uptake of gold nanoparticles: what we have learned so far?." *Journal of nanoparticle research : an interdisciplinary forum for nanoscale science and technology* vol. 12,7 (2010): 2313-2333. doi:10.1007/s11051-010-9911-8

[7] Cedervall, T., Lynch, I., Foy, M., Berggard, T., Donnelly, S., Cagney, G., Linse, S., and Dawson, K., "Detailed Identification of Plasma Proteins Adsorbed on Copolymer Nanoparticles." *Angewandte Chemie International Edition*, vol. 46, no. 30, 2007, pp. 5754–56. *Crossref*, doi:10.1002/anie.200700465.

[8] Aggarwal, P., Hall, J., McLeland, C., Dobrovolskaia, M., and McNeil, S., "Nanoparticle interaction with plasma proteins as it relates to particle biodistribution, biocompatibility and therapeutic efficacy." *Advanced drug delivery reviews* vol. 61,6 (2009): 428-37. doi:10.1016/j.addr.2009.03.009

[9] Kutz, M., Adrezin, R., Barr, R., Batich, C., Bellamkonda, R., Brammer, A., Buchanan, T., Cook, A., Currie, J., and Dolan, A., (2003). *Standard handbook of biomedical engineering and design.*2003

[10] White, Frank. *Viscous Fluid Flow (MCGRAW HILL SERIES IN MECHANICAL ENGINEERING)*. 3rd ed., McGraw-Hill Education, 2005.

[11] Formaggia, L., Lamponi, D., and Quarteroni, A. "One-Dimensional Models for Blood Flow in Arteries." *Journal of Engineering Mathematics*, vol. 47, no. 3/4, 2003, pp. 251–76. *Crossref*, doi:10.1023/b:engi.0000007980.01347.29.

[12] Ghigo, A. R., Lagree, P.Y., and Fullana J.M. "A Time-Dependent Non-Newtonian Extension of a 1D Blood Flow Model." *Journal of Non-Newtonian Fluid Mechanics*, vol. 253, 2018, pp. 36–49. *Crossref* doi:10.1016/j.jnnfm.2018.01.004.

[13] Einstein, A., 1906, "A New Determination of the Molecular Dimensions," Ann. Phys., 19(2), pp. 289–306.

[14] de Bruijn, H., 1942, "The Viscosity of Suspensions of Spherical Particles. (The fundamental η-c and φ relations)" Recl. Trav. Chim. Pays-Bas, 61(12),pp. 863–874.

[15] Vand, V., 1948, "Viscosity of Solutions and Suspensions. I. Theory," J. Chem. Phys., 52(2), pp. 277–299.

[16] Mooney, M., 1951, "The Viscosity of a Concentrated Suspension of Spherical Particles," J. Colloid Sci., 6(2), pp. 162–170.

[17] Brinkman, H. C., 1952, "The Viscosity of Concentrated Suspensions and Solutions," J. Chem. Phys., 20(4), pp. 571–581.

[18] "Introduction." *Atherosclerosis*, Boston University School of Public Health, sphweb.bumc.bu.edu/otlt/mph-modules/ph/ph709_heart/ph709_heart_print.html.

[19] Claes, E, Atienza, J.M., Guinea, C.V., Rojo, F.J., Bernal, J.M., Revualta, J.M., and Elices, M. "Mechanical Properties of Human Coronary Arteries." *2010 Annual International Conference of the IEEE Engineering in Medicine and Biology*, 2010, doi:10.1109/iembs.2010.5627560.

[20] Okamoto, Ruth J., Wagenseil, Jessica E., DeLong, William R., Peterson, Sara J., Kouchoukos, Nicholas T., and Sundt, Thoralf M. "Mechanical Properties of Dilated Human Ascending Aorta." *Annals of Biomedical Engineering*, vol. 30, no. 5, 2002, pp. 624–635., doi:10.1114/1.1484220.

Chapter 2: Viscosity of Blood Like Fluid

2.1 Viscosity Equations

A value for blood viscosity is required in order to develop a flow model for blood through the aortic arch. Although blood is known to be a non-Newtonian fluid, in many preliminary studies it is modeled as a Newtonian fluid when it is flowing through a large main artery. The flow also is an average blood velocity rather than the actual pulsatile flow found in the human body. Viscosities from 30 degrees Celsius to 40 degrees Celsius were used in the model using the following equation for determining viscosities of a blood-like fluid based on temperature in degrees Celsius [1]:

$$\mu = 0.0041T^2 - 0.3318T + 9.6544 \tag{18}$$

This equation was developed by Yousif, Holdsworth, and Poepping [1] who synthesized a blood mimicking fluid and experimentally determined viscosity, μ, in centipoise, of the fluid at temperatures between 20 and 27 deg C. Figure 11 shows their experimental results. The dashed line shows viscosity and the solid line is the refractive index for the Blood Mimicking Fluid (BMF). The following is the equivalent of centipoise (cP) in terms of SI units.

$$1\,poise\,(P) = 1\frac{g}{cm * s} = 100\,cP = 0.1\frac{kg}{m * s}$$

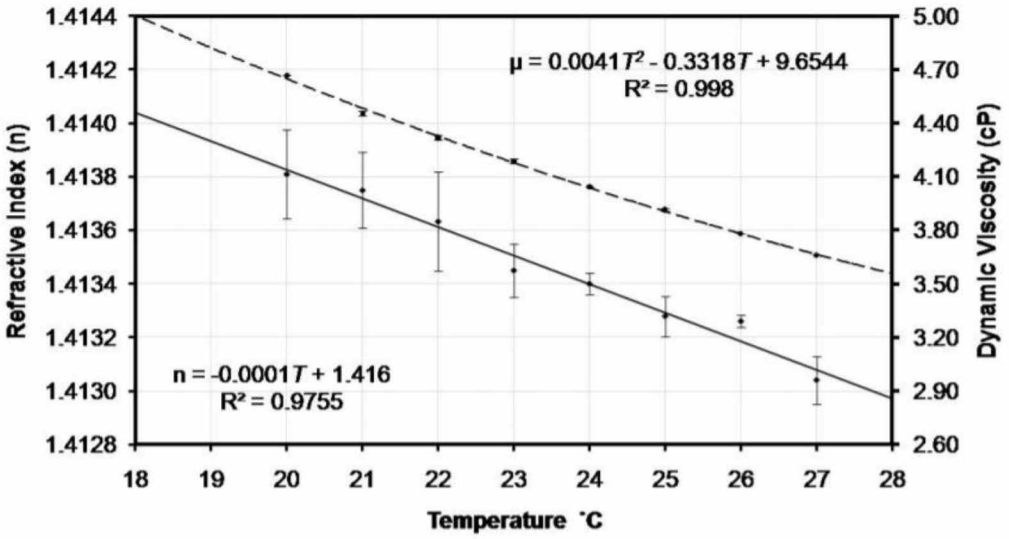

Figure 11:Experimental results for viscosity of a blood mimicking fluid [1]

Viscosities of the BMF between 30 and 40 degrees Celsius are tabulated below.

Table 1: Viscosities of a blood mimicking fluid from 30 to 40 degrees Celsius

T (°C)	μ (cP)
30	3.3904
31	3.3087
32	3.2352
33	3.1699
34	3.1128
35	3.0639
36	3.0232
37	2.9907
38	2.9664
39	2.9503
40	2.9424

The blood mimicking fluid developed by earlier researchers is a mixture of water, glycerol, and sodium iodide. Glycerol is chemically very similar to ethylene glycol. Equations that have been developed for viscosity of ethylene glycol based nanofluids are appropriate to implement here. In 2007, Namburu, Kulkarni, Misra, and Das [2] experimentally determined the correlation for an ethylene glycol based nanofluid to be the following based on the volume concentration (ϕ) :

$$log(\mu_{eff}) = Ae^{-BT} \quad (19)$$

The temperature of the nanofluid, T, is in Kelvin. The values for A and B are functions of volume concentration as shown in equations 20 and 21.

$$A = 1.8375\phi^2 - 29.643\phi + 165.56 \quad (20)$$

$$B = 4.8 * 10^{-6}(\phi)^2 - 0.001\phi + 0.0186 \quad (21)$$

In 2009, Sahoo et al. [3] extended the temperature range of viscosity measurements and updated the viscosity correlation to:

$$\mu_{nf} = Ae^{\left(\frac{B}{T}+C\phi\right)} \quad (22)$$

A, B, and C are not functions of volume concentration, but constants based on the temperature range of the nanofluid in Kelvin. The figure below shows the experimental data used to determine these constants.

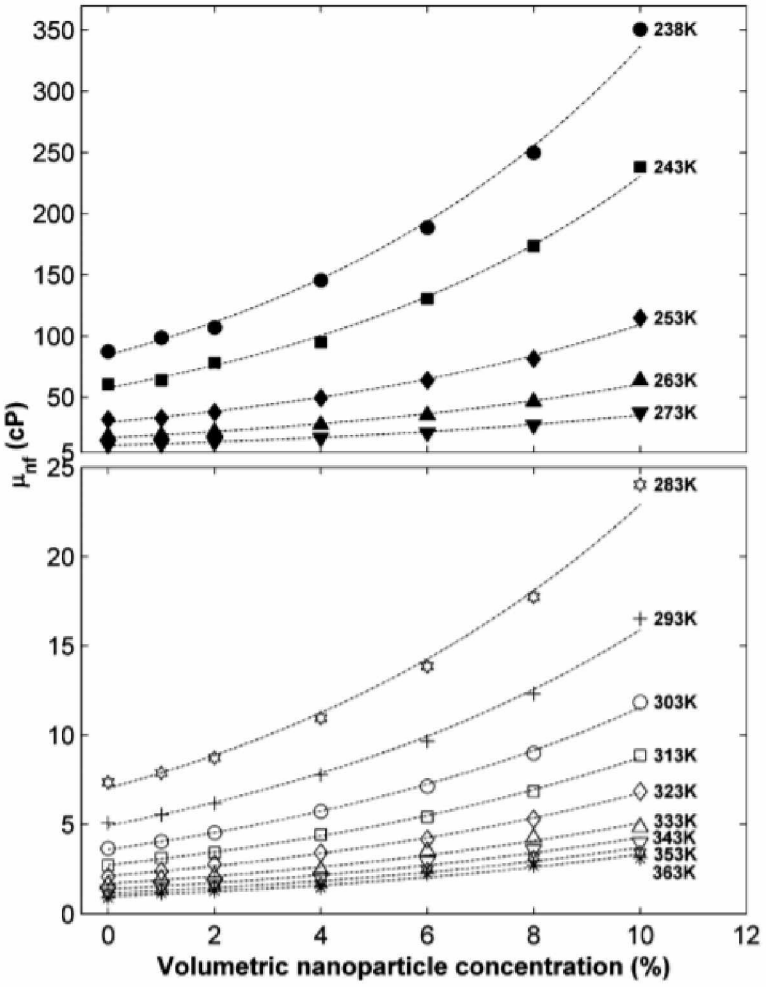

Figure 12:Experimental data for nanofluid viscosity [3]

The Table 2 defines the values of A, B, and C for the 2 temperature ranges developed by Sahoo et al.

Table 2: Variable values for Equation 22 in high and low temperature ranges [3]

Variable	Low Range (238-273 K)	High Range (273-363 K)
A	$1.2200 * 10^{-6}$	$2..3920 * 10^{-4}$
B	4285	2903
C	0.1448	0.1265
R^2	0.9984	0.9958

In 2009, Vajjha, Das, and Namburu [4] further improved the viscosity correlation by non-dimensionalizing the viscosities of the nanofluid and the base fluid. The results are shown in Equation 23.

$$\frac{\mu_{nf}}{\mu_{bf}} = Ae^{(C\phi)} \tag{23}$$

The values for A and C in Equation 23 are constants determined by the type of nanofluid under examination. Since the effect of gold nanoparticles on the viscosity of an glycerol based blood mimicking fluid is being examined, and the chemical makeup of glycerol is very similar to that of ethylene glycol, the correlation developed by Vajjha, Das, and Namburu was selected to examine gold nanoparticle effects on the viscosity of the blood mimicking fluid. The constants A and C for Aluminum Oxide were used as a first approximation for these calculations because no constants for gold nanoparticles were available in the literature. The values for A and C are 0.983 and 12.959 respectively. In the future, gold nanoparticles should be dispersed in the BMF and viscosity measurements should be made to improve predictions.

2.2 Blood Mimicking Fluid Viscosity Calculations

The equation developed by Vajjha, Das, and Namburu [4] was applied to calculated values for blood mimicking fluid viscosity from 30 to 40 degrees Celsius. Table 3 shows the effects of nanoparticle introduction to blood viscosity.

Table 3: Viscosity of Blood Mimicking Fluid with gold nanoparticles at varied concentrations

T (Celsius)	Base Fluid cP	1% Gold cP	2% Gold cP	3% Gold cP	4% Gold cP	5% Gold cP
30.000	3.390	3.794	4.319	4.916	5.597	6.371
30.500	3.349	3.747	4.265	4.856	5.527	6.292
31.000	3.309	3.702	4.215	4.798	5.462	6.217
31.500	3.271	3.660	4.167	4.743	5.399	6.146
32.000	3.235	3.620	4.121	4.691	5.340	6.079
32.500	3.202	3.583	4.078	4.642	5.285	6.016
33.000	3.170	3.547	4.038	4.597	5.233	5.957
33.500	3.140	3.514	4.000	4.554	5.184	5.901
34.000	3.113	3.483	3.965	4.514	5.138	5.849
34.500	3.087	3.455	3.933	4.477	5.096	5.801
35.000	3.064	3.429	3.903	4.443	5.058	5.757
35.500	3.043	3.405	3.876	4.412	5.022	5.717
36.000	3.023	3.383	3.851	4.384	4.990	5.681
36.500	3.006	3.364	3.829	4.359	4.962	5.648
37.000	2.991	3.347	3.810	4.337	4.937	5.620
37.500	2.978	3.332	3.793	4.318	4.915	5.595
38.000	2.966	3.319	3.779	4.302	4.897	5.574
38.500	2.957	3.309	3.767	4.288	4.882	5.557
39.000	2.950	3.301	3.758	4.278	4.870	5.544
39.500	2.945	3.296	3.752	4.271	4.862	5.535
40.000	2.942	3.293	3.748	4.267	4.857	5.529

As expected, the introduction of gold nanoparticles to the fluid significantly increases viscosity as the concentration increases from 0% to 5%. At a concentration of 5%, the calculated viscosity is almost double that of the base fluid by itself. Note that a concentration of 5% would likely not be introduced into a patient. Since it's been shown that gold nanoparticles of any size will accumulate in the internal organs of the host (including the brain if the particles are small enough), any amount of gold nanoparticles introduced to a patient for therapeutic purposes would be of negligible concentration. Figure 13 gives a visual representation of the variation in viscosity with an increase in temperature and nanoparticle volumetric concentration. Most liquids display a characteristic of diminishing viscosity with an increase in temperature. This gold nanofluid is also displaying the same behavior in Figure 13.

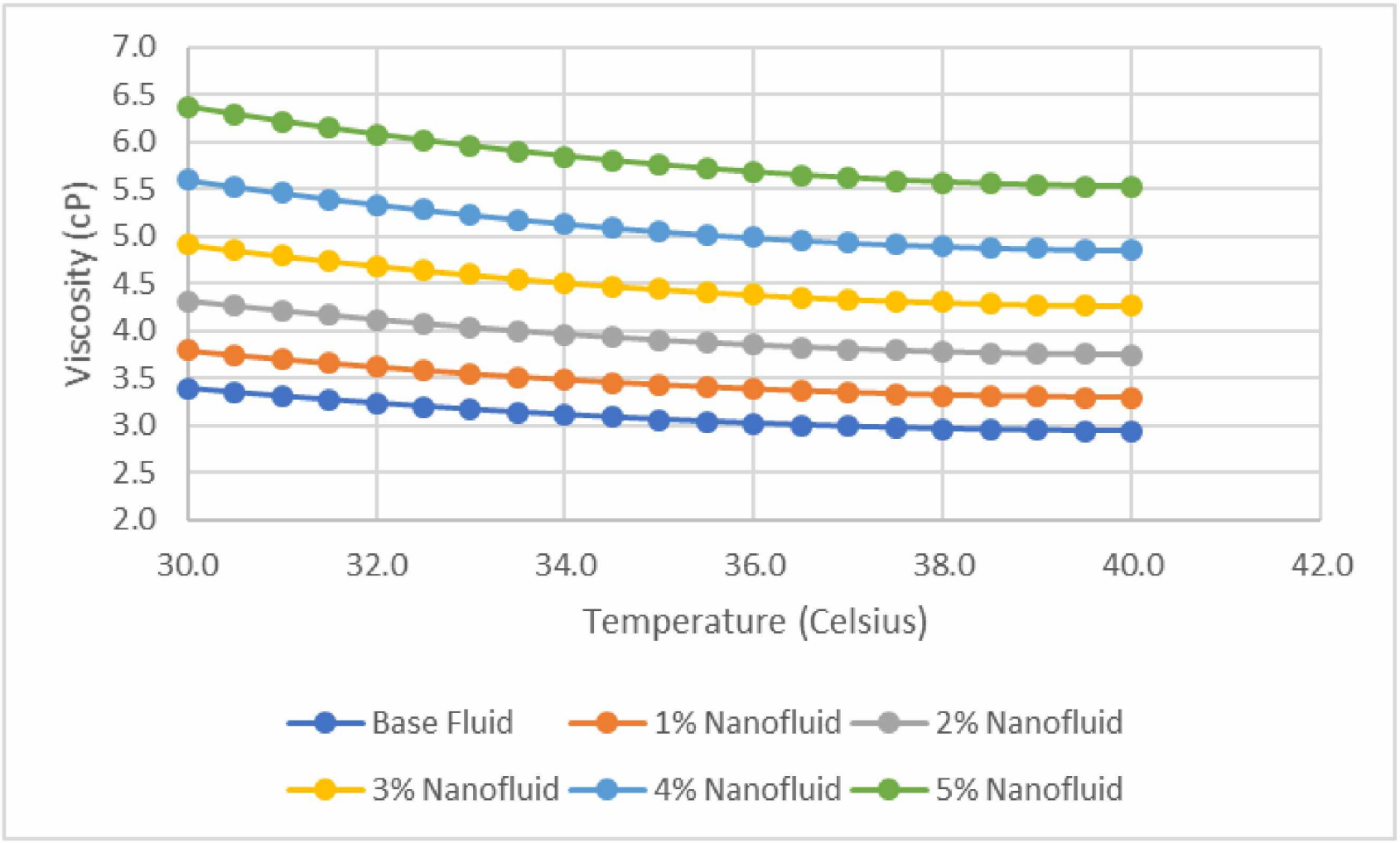

Figure 13:Viscosity vs Temperature of Blood Mimicking Fluid for 0-5% volume concentration

2.3 References

[1] Yousif, Majid Y., David W. Holdsworth, and Tamie L. Poepping. "A blood-mimicking fluid for particle image velocimetry with silicone vascular models." *Experiments in fluids* 50.3 (2011): 769-774.

[2] Namburu, Praveen & Kulkarni, Devdatta & Misra, Debasmita & Das, Debendra. (2007). Viscosity of copper oxide nanoparticles dispersed in ethylene glycol and H2O mixture. Experimental Thermal and Fluid Science. 32. 397-402. 10.1016/j.expthermflusci.2007.05.001.

[3] Sahoo, B. C., Vajjha, R., Ganguli, R., Chukwu, G., Das, D. "Determination of Rheological Behavior of Aluminum Oxide Nanofluid and Development of New Viscosity Correlations." *Petroleum Science and Technology*, vol. 27, no. 15, 2009, pp. 1757–70. *Crossref*, doi:10.1080/10916460802640241.

[4] Vajjha, Ravikanth S., Das, D., Namburu, P. "Numerical Study of Fluid Dynamic and Heat Transfer Performance of Al2O3 and CuO Nanofluids in the Flat Tubes of a Radiator." *International Journal of Heat and Fluid Flow*, vol. 31, no. 4, 2010, pp. 613–21. *Crossref*, doi:10.1016/j.ijheatfluidflow.2010.02.016.

Chapter 3: Computational Modeling of Nanofluid Flow

3.1 Model Equations

Using the governing equations provided in Equations 3-6 listed under Section 1.4, ANSYS Fluent CFD Code Version 19.1 was used to model nanofluid flow through the aorta. The density was supplied to the code via the nanofluid equation provided by Pak and Choi [1].

$$\rho_{nf} = \rho_{bf}(1 - \phi) + \rho_p \phi \tag{23}$$

ρ_{nf} is the density of the nanofluid, ρ_{bf} is the density of the base fluid, ϕ is volumetric concentration, and ρ_p is the density of the particle. The density of gold is known to be 19300 $\frac{kg}{m^3}$ and the density of blood is known to be about 1025 $\frac{kg}{m^3}$ [2]. The viscosity was provided to the simulation from Table 3 presented in Chapter 2.

3.2 Aorta Geometry

The geometry for the aortic arch is a 2-dimensional construct that captures the entering flow region coming from the heart, three exit flow regions at the top of the aortic arch that represent the subclavian and carotid arteries, and the main exit flow region of the descending aorta. A survey of anatomy references was conducted, and a wide variety of values for the diameters of each section is reported. The following set of values was used as they fell well within the minimum and maximum values in the existing data available [3] [4]:

Table 4: Diameters used in the model for the various arterial branches

Area	Diameter (mm)
Left Subclavian Artery	9.04
Left Carotid Artery	7.15
Brachiocephalic Artery	12.07
Ascending Aorta	32.58
Aortic Arch Width (center to center)	79.00

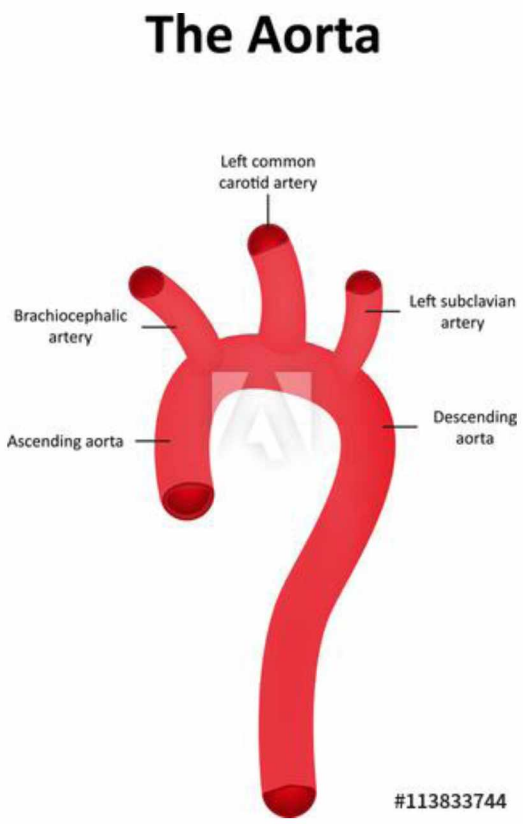

Figure 14:Image of the aortic arch and related arteries [5]

The area being modeled starts above the coronary arteries, covers the entire arch including the three main artery branches on the top, and down the descending aorta to a point even with the starting point. The preliminary selection of this geometry can be improved to refine the CFD model so that it can then be applied to more complex geometries. The surface properties applied to the aorta walls was simply a no-slip boundary condition on solid surfaces. The inlet boundary condition is a uniform velocity and pressure, and the outlet boundary condition used in the model was the percentage of output flow through each outgoing flow boundary. The values shown in Table 5 were derived from outlet conditions determined in previous research of a larger section of the aorta [6].

Table 5:Flow rate ratings for each flow output location

Outflow Location	Flow Rate Weighting
Brachiocephalic Artery	0.15
Left Subclavian Artery	0.075
Left Carotid Artery	0.075
Descending Aorta	0.70

Once all of these input parameters were entered into the ANSYS Fluent model, cases were run for the base fluid viscosity from 30 to 40 degrees Celsius in 1-degree Celsius increments. The computations produced velocity contours and velocity vector results, which are discussed subsequently.

3.3 Results

Using the post processing capability of ANSYS Fluent, graphics showing the velocity contours and the velocity vector fields were generated for each temperature listed in Table 3. Some results are highlighted here. However, each case is provided in Appendix A. Figure 15 below shows the initial results based on a crude mesh used with a viscosity value of 4.4 cP, which can represent 3% nanofluid at 35 degrees Celsius. This first run showed large areas with very little flow. This may be due to the incorrect selection of computational domain. The 3 branch arteries are modeled too short so that flow does not get a chance to be fully developed in them, whereas in actual cases the branches are long enough to produce fully developed flows.

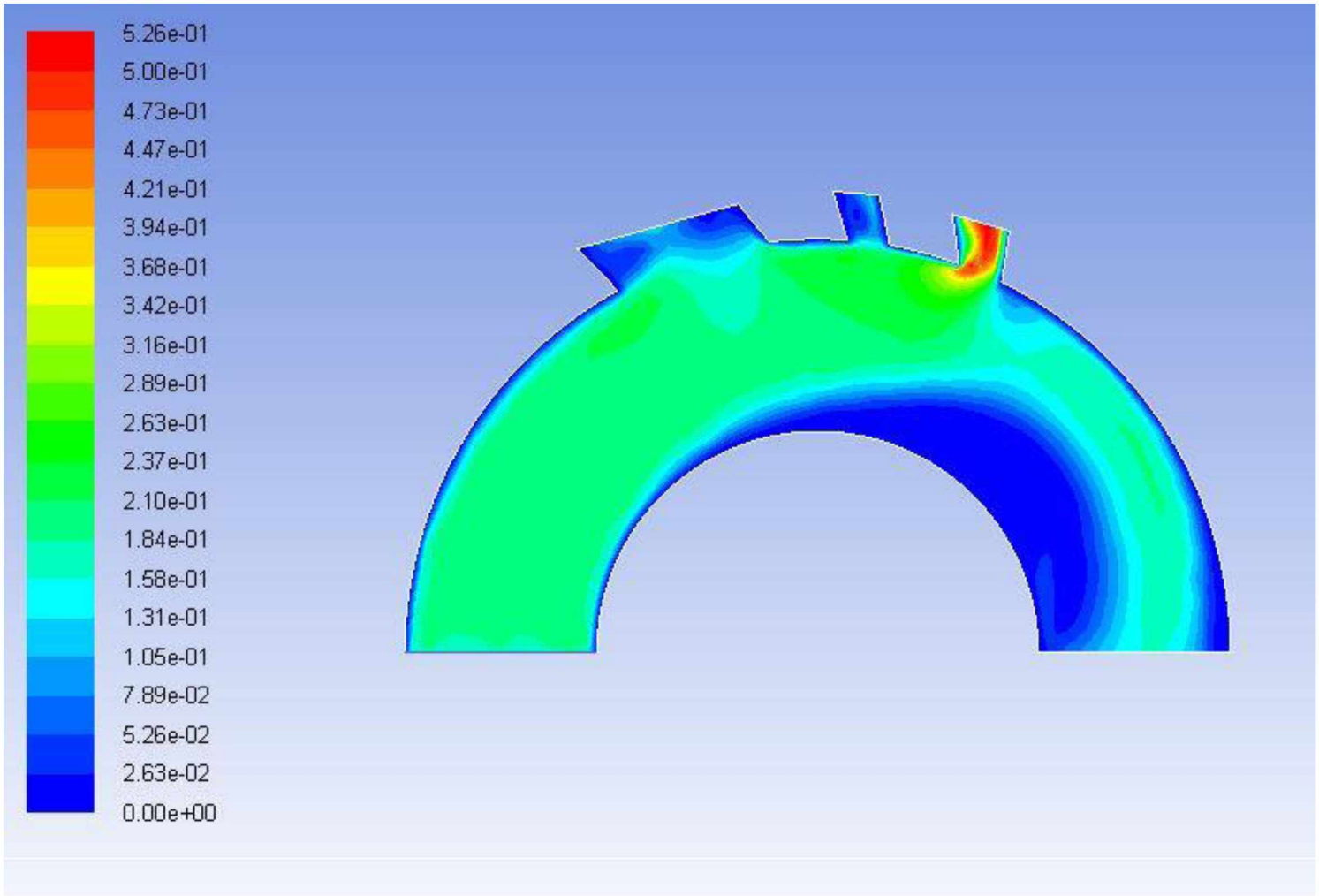

Figure 15:First case run with initial geometry and crude mesh showing velocity contours. The velocity scale is in meters per second.

A viscosity using Equation 18 was applied to a second run with a more refined mesh and with the branching arteries elongated to provide space for the flow to fully develop. Figure 16 shows the resulting velocity contour. Once the model parameters were settled, the cases from 30 to 40 degrees Celsius were all run in 1-degree Celsius increments. Figures 17-20 show the velocity contours and vector fields for viscosities at 30 degrees Celsius and 40 degrees Celsius for comparison. Most of the velocity profiles remained very similar across the range of temperatures and viscosities. Small changes in the shape of the velocity contours are evident when a graphic is created that runs through each case. The velocity values tend towards the bottom end of spectrum due to using an average rate of blood flow rather than pulsatile flow, where peaks of up to 120 cm/s have been measured [7]. The velocity vector fields were of particular interest. Where the velocity contours may show an area where flow is approaching negligibly small velocity, the velocity vector field shows more clearly what is occurring. Figure 21 clearly shows an area of recirculation inside the Brachiocephalic artery where gold nanoparticles may congregate. These are areas to be further scrutinized when trying to determine how the gold nanoparticles will be affected by the motion of the blood.

The simulations presented in this study are for entry Reynolds numbers in the neighborhood of 700. Therefore, all the models are for laminar flow conditions. These velocity distribution diagrams prove that blood will accelerate (along with nanoparticles) to reach highest velocity magnitude in a region just prior to the entrance to the Brachiocephalic artery.

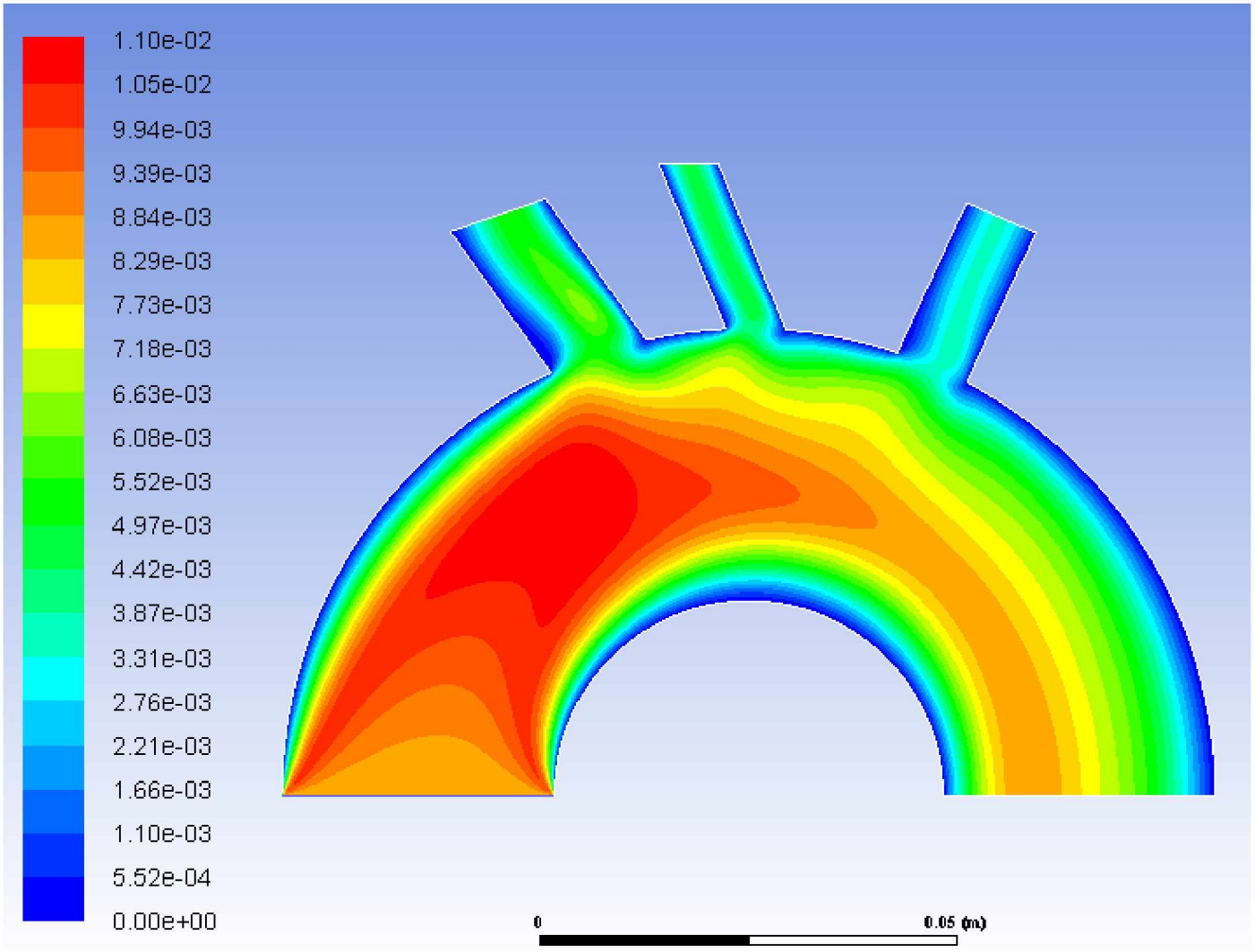

Figure 16: Elongated arteries and refined mesh

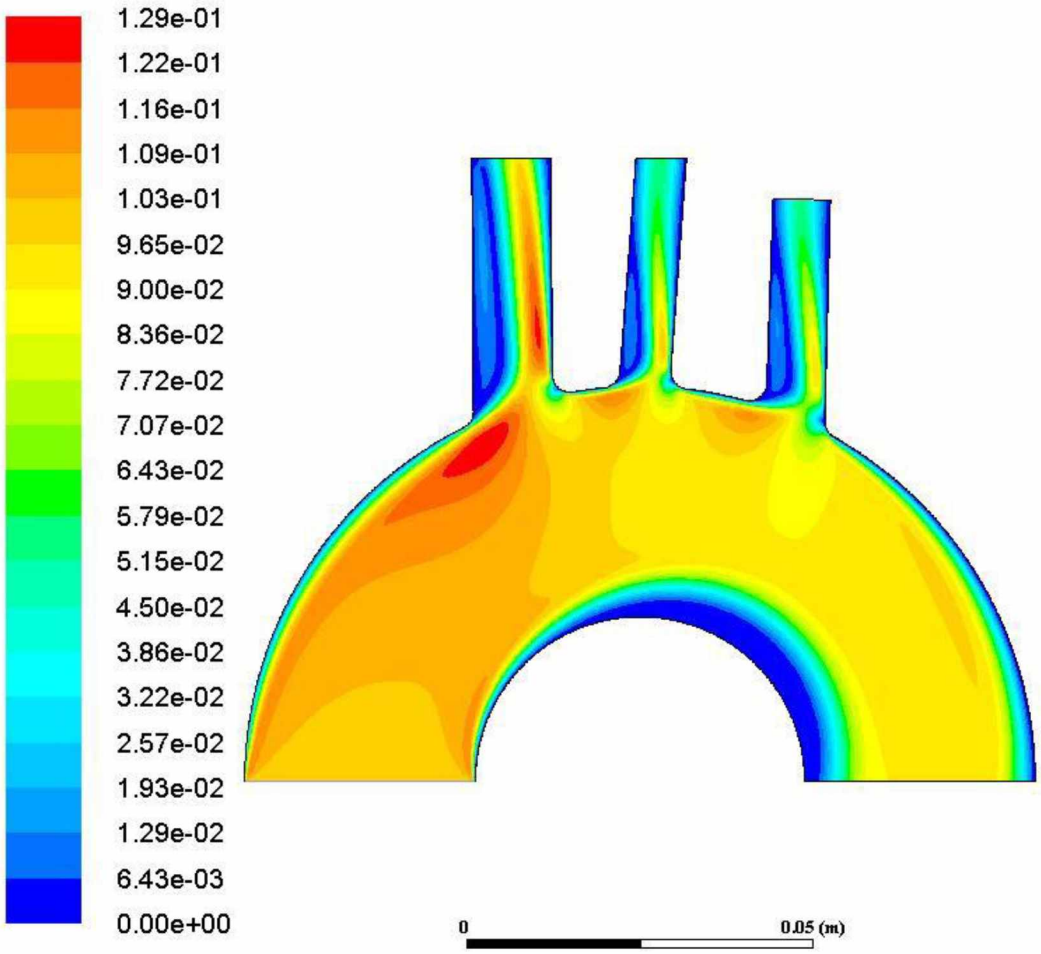

Figure 17: Velocity contours at 30 degrees Celsius

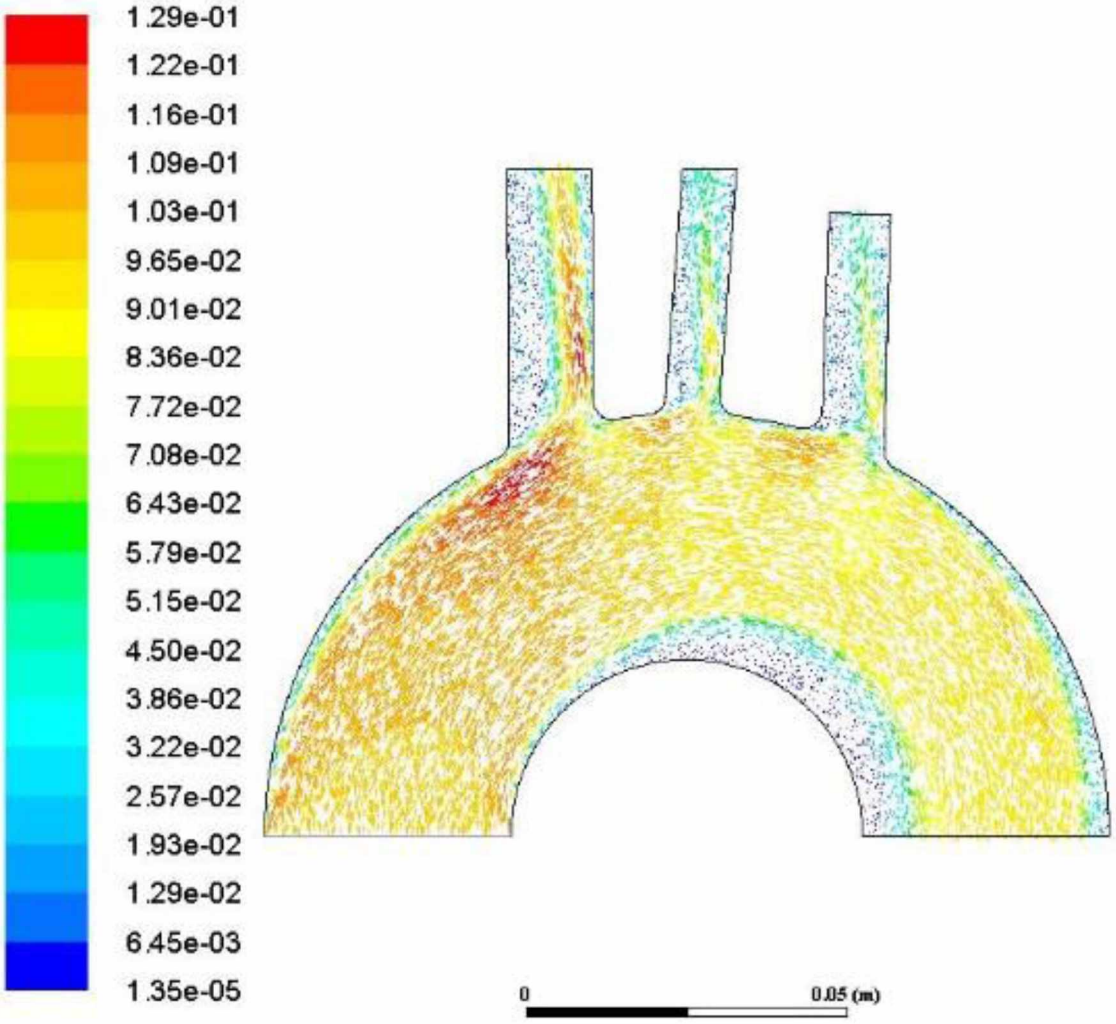

Figure 18: Velocity vector field at 30 degrees Celsius

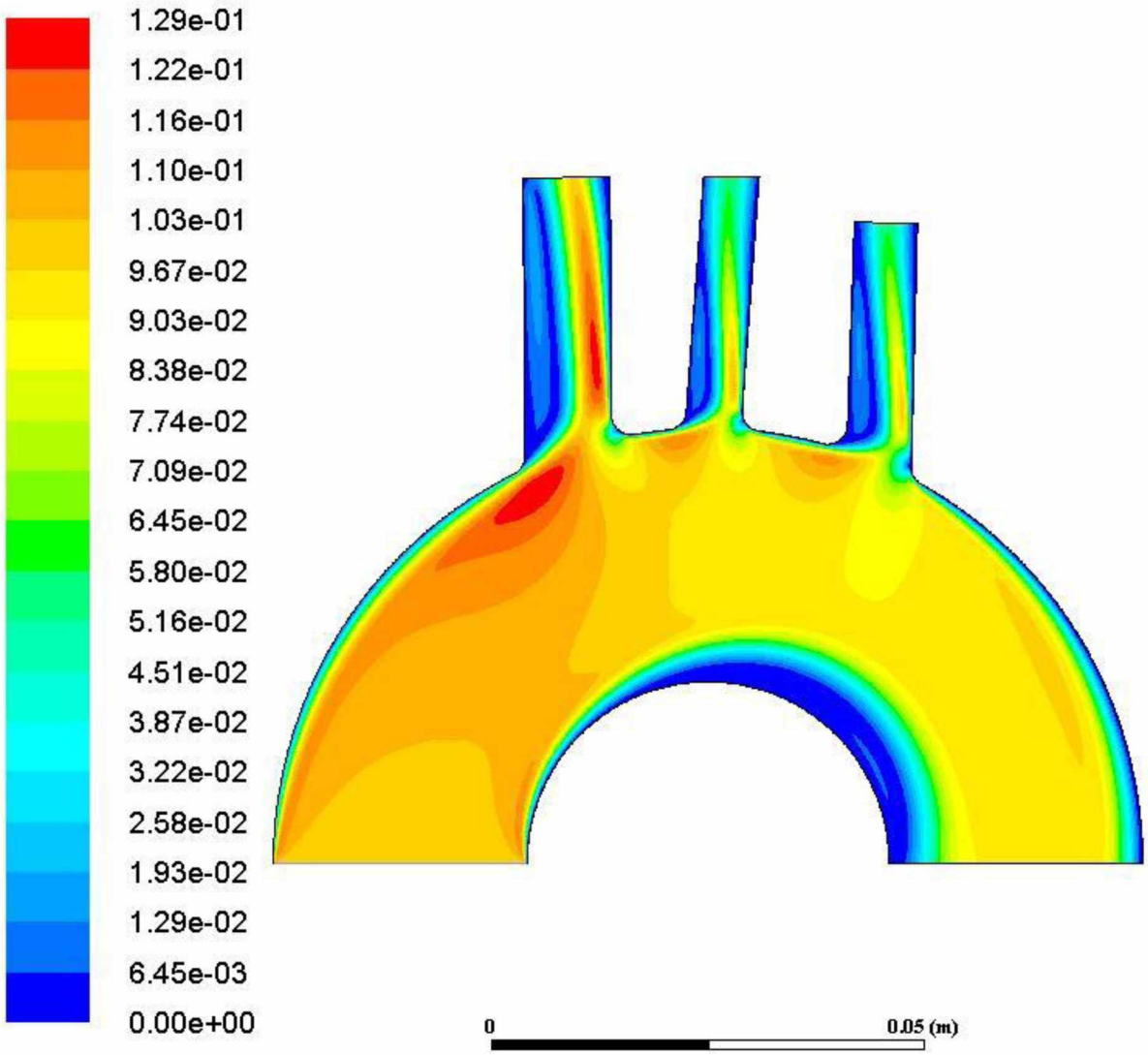

Figure 19: Velocity contour at 40 degrees Celsius

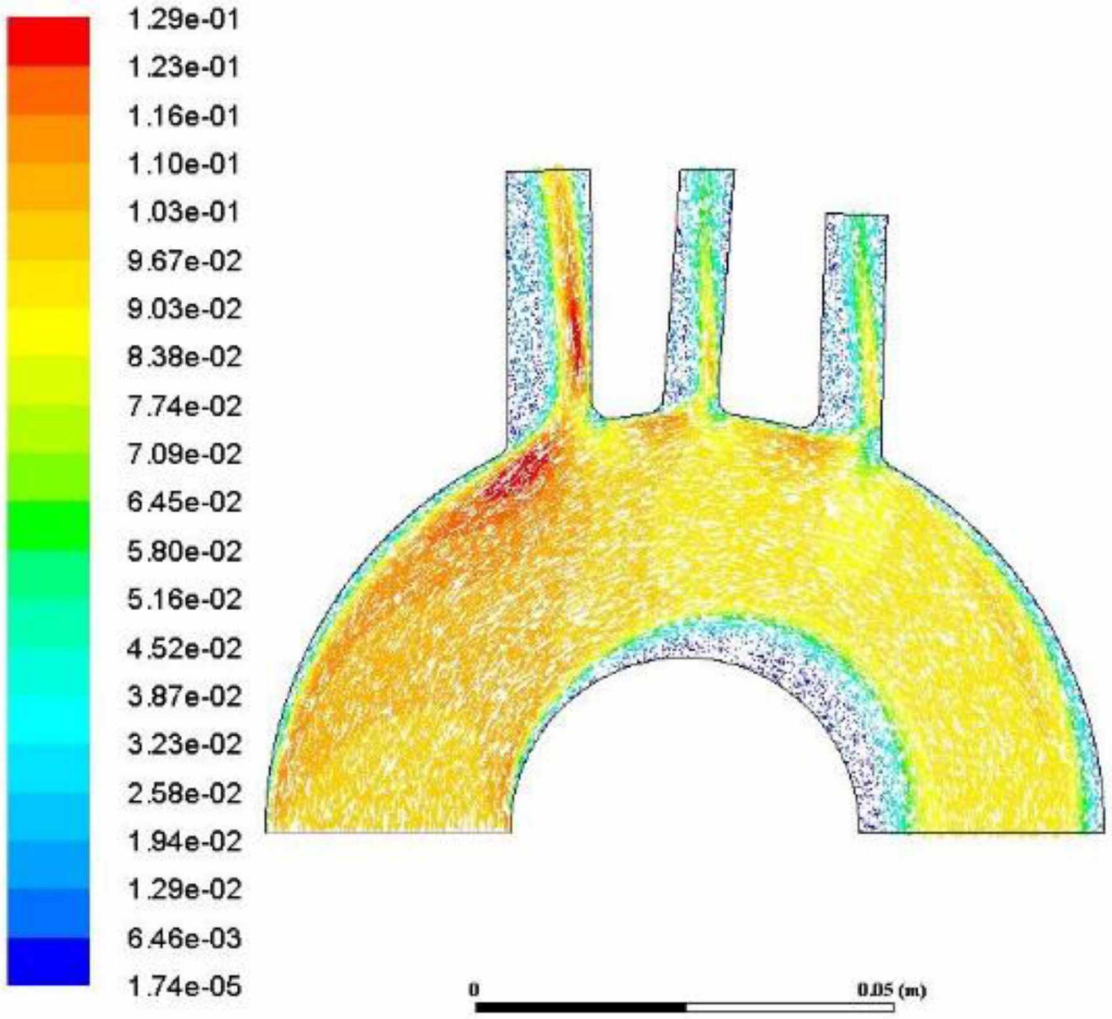

Figure 20:Velocity vector field at 40 degrees Celsius

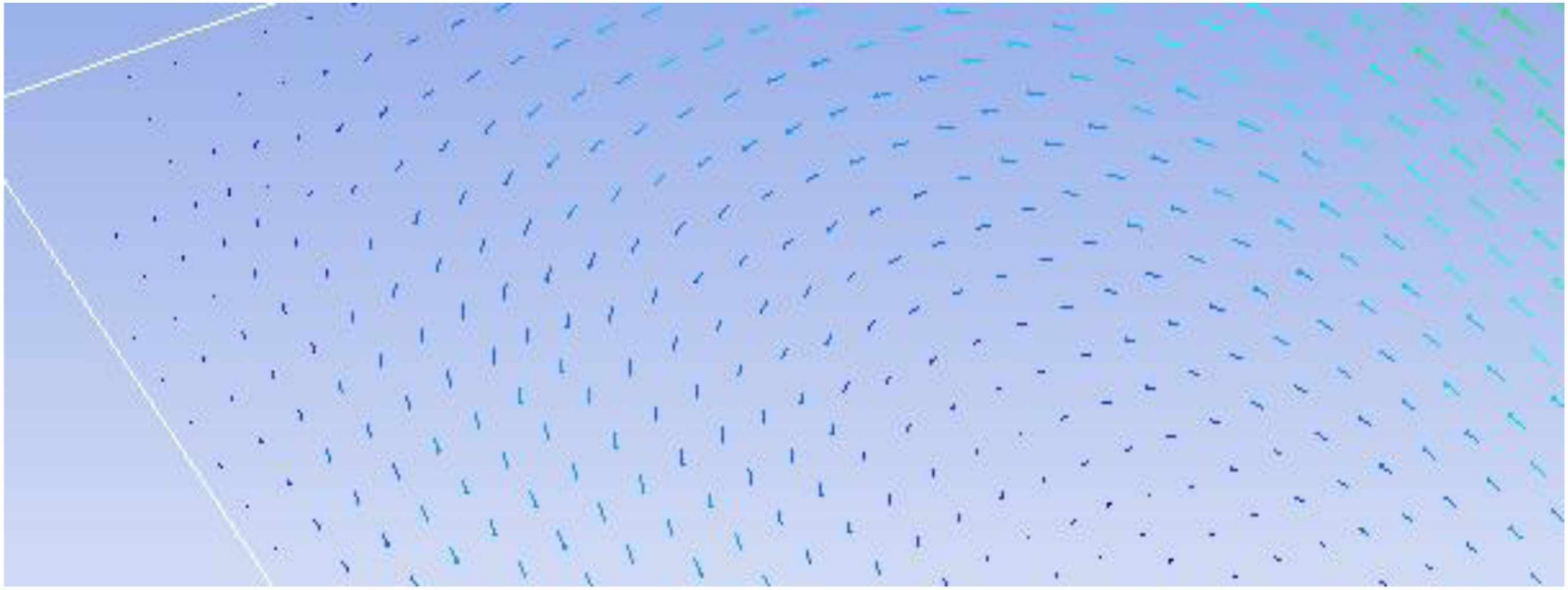

Figure 21: Close up view of velocity vector field in Brachiocephalic artery at 40 degrees Celsius showing recirculation.

3.4 References

[1] Pak, B. C., and Cho, Y. I., "Hydrodynamic and Heat Transfer Study of Dispersed Fluids With Submicron Metalic Oxide Particles," *Exp. Heat Transfer*, 1998 11(2), pp. 151–170.

[2] Elert, Glenn. "Density of Blood." *Density of Blood- The Physics Factbook*, 2004, hypertextbook.com/facts/2004/MichaelShmukler.shtml.

[3] Chuang, Michael L., Gona P., Musgrave, R., Qazi, S., Fox, C., Massaro, J., Hoffmann, U., and O'Donnell, C. "Abstract P372: Increased Aortic Arch Width is an Independent Predictor of Incident Adverse Cardiovascular Disease Events: The Framingham Heart Study." (2015).

[4] Kahraman, H., Ozaydin, M., Varol, E., Aslan, S., Dogan, A., Altinbas, A., Demir, M., Gedikli, O., Acar, G., and Ergene, O. "The diameters of the aorta and its major branches in patients with isolated coronary artery ectasia." *Texas Heart Institute Journal* 33.4 (2006): 463.

[5] "The Aorta Labeled Diagram." *Adobe Stock*, Adobe, stock.adobe.com/nl/images/the-aorta-labeled-diagram/113833744?as_campaign=ftmigration2&as_channel=dpcft&as_campclass=brand&as_source=ft_web&as_camptype=acquisition&as_audience=users&as_content=closure_asset-detail-page. Accessed 11 Mar. 2020.

[6] Benim, A. C., Nahavandi, A., Assmann, A., Schubert, D., Feindt, P., and Suh, S. "Simulation of blood flow in human aorta with emphasis on outlet boundary conditions." *Applied Mathematical Modelling* 35.7 (2011): 3175-3188.

[7] Gisvold, S. E., and A. O. Brubakk. "Measurement of instantaneous blood-flow velocity in the human aorta using pulsed Doppler ultrasound." *Cardiovascular research* 16.1 (1982): 26-33.

Chapter 4: Conclusion and Recommendations

4.1 Conclusion

Gold nanoparticles show great promise in the biomedical field as a way to increase certain cancer treatment efficiencies [1]. Before these nanoparticles can be deployed in a patient's body, the behavior of these nanoparticles in the blood stream will need to be understood and predicted. Although gold is a relatively stable element, on a nanoscale these particles will infiltrate internal organs including the brain. Functionalizing the nanoparticle and bonding it with antibodies is a possible avenue of controlling behavior of these nanoparticles, but an effective method of removing these particles from the body would be required. Developing a model of blood flow through the body is a first step in being able to understand how gold nanoparticles will behave in the body and to deploy these particles for medical reasons. It is evident from these preliminary results that there are areas of recirculation in the blood flow where gold nanoparticles could potentially congregate.

Equations have been developed to predict how nanoparticles change the thermophysical properties of a fluid. This has been extensively studied in water, and propylene glycol/water and ethylene glycol/water mixtures. These equations can be applied to blood to see what effect these particles will have on the intrinsic fluid properties of blood. The focus here was on viscosity, and it was demonstrated that viscosity will increase with the addition of nanoparticles as expected.

4.2 Recommendations

This set of models is a good initial step to creating an accurate model of blood flow with gold nanoparticles through the aortic arch. Areas of possible recirculation have been identified and general velocity profiles and vector fields have been generated. However, there are quite a few improvements that need to be made in order to create a more accurate model.

In this case, only viscosity was changed in order to define the fluid properties of the model. Values of specific heat, thermal conductivity, and density should be determined for the temperature range and applied to the fluid properties in the model. A data set describing these properties for blood over a temperature range is not currently readily available. Known

correlations for properties of water, propylene glycol, and ethylene glycol can be used in the next round of simulations as starting points. In addition to the fluid properties being refined in the model, the non-Newtonian properties of blood can be incorporated into the model. The pulsatile nature of blood flow can also be incorporated into the model by modeling the unsteady governing equations. The energy conservation should be added to the modeling to take temperature effect into account.

In addition to improvements to the fluid properties of the system, the properties of the aorta wall should be updated. The aorta wall is not a solid no-slip surface. It is a complicated biological system that may impact how the blood flows through the aorta. Another step that should be taken is creating a 3-dimensional model of the aorta itself and run simulations with the refined boundary conditions and fluid properties.

Further study is required to understand how gold nanoparticles will affect the body. In spite of the fact that gold nanoparticles of a certain size may not be toxic to a patient, even a 1% volume concentration in the blood system would lead to serious complications as the nanoparticles migrate to internal organs and become embedded. The human body has a threshold of tolerance for foreign objects. Research should be done to determine what concentration of gold nanoparticles can be tolerated by the human body. Part of this study should be research into how these nanoparticles can be efficiently extracted from the body once they are no longer required. We also need an understanding of how modified properties of blood due to the introduction of nanoparticles to the system will affect the health of a patient.

There has been extensive research conducted in understanding how nanoparticles affect the thermophysical properties of a fluid. This area of research should be expanded to include nanoparticles that could be used for therapeutic medical applications and how they affect the thermophysical properties of blood.

This area of research is multidisciplinary. Not any one field will be able to answer all of the questions when it comes to how nanoparticles can be used on human patients. However, it is definitely worth pursuing as any tool in the fight against cancer is extremely important.

4.3 References

1] Antosh, M. P., Wijesinghe, D. D., Shrestha, S., Lanou, R., Huang, Y. H., Hasselbacher, T., Fox, D., Neretti,N., Sun, S., Katenka, N., Cooper, L. N., Andreev, O. A., and Reshetnyak, Y. K., 2015, "Enhancement of radiation effect on cancer cells by gold-pHLIP," Proceedings of the National Academy of Sciences, 112(17), pp. 5372-5376.

Appendix A

Appendix A contains the results of 20 ANSYS Fluent computational runs. The results appear in order starting from a fluid temperature of 30 degrees Celsius and ending at 40 degrees Celsius. There are 2 sets for each temperature. The first is the velocity contour plot, and the second is the velocity vector field.

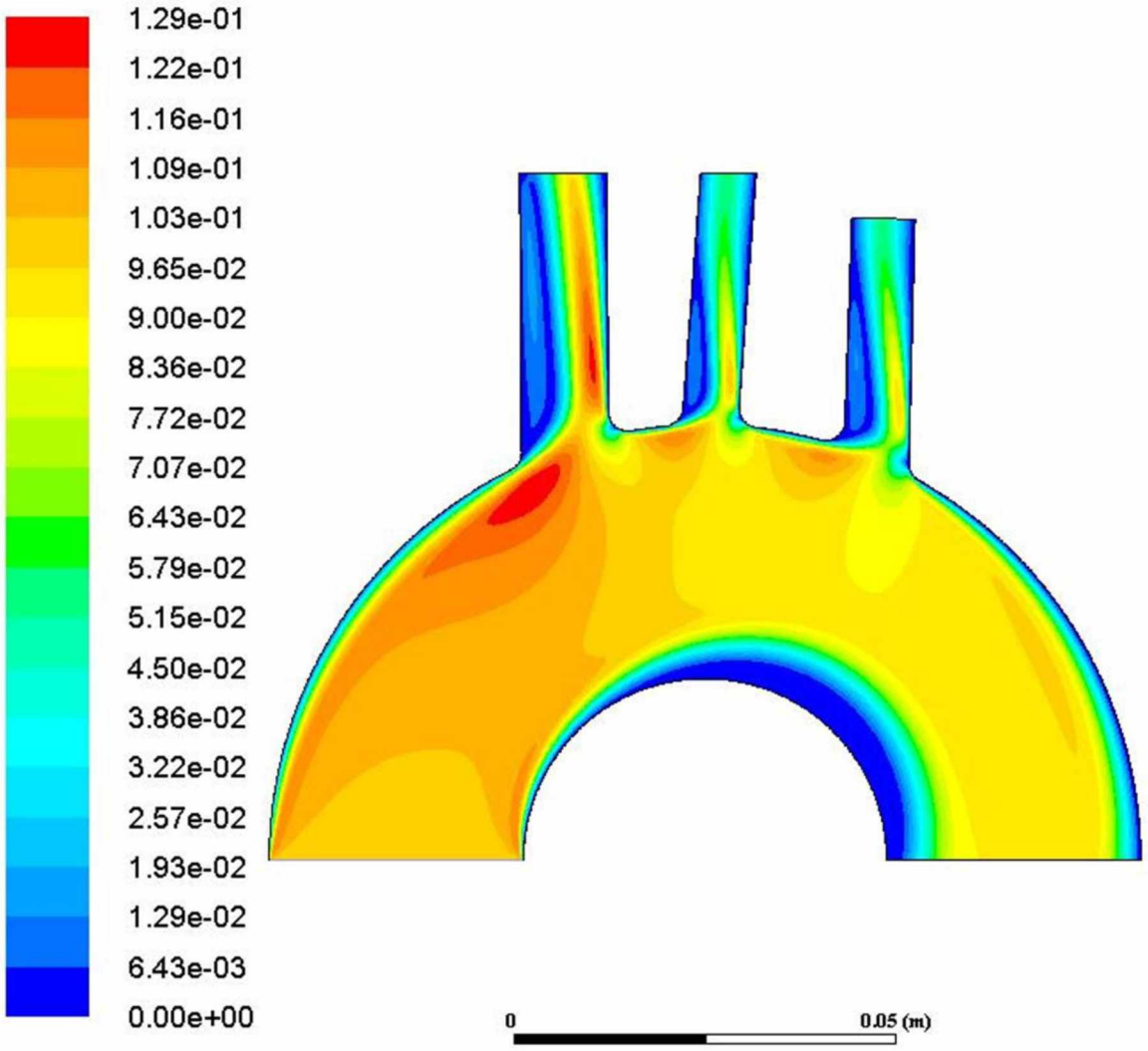

Figure 22: Velocity contour at 30 degrees Celsius

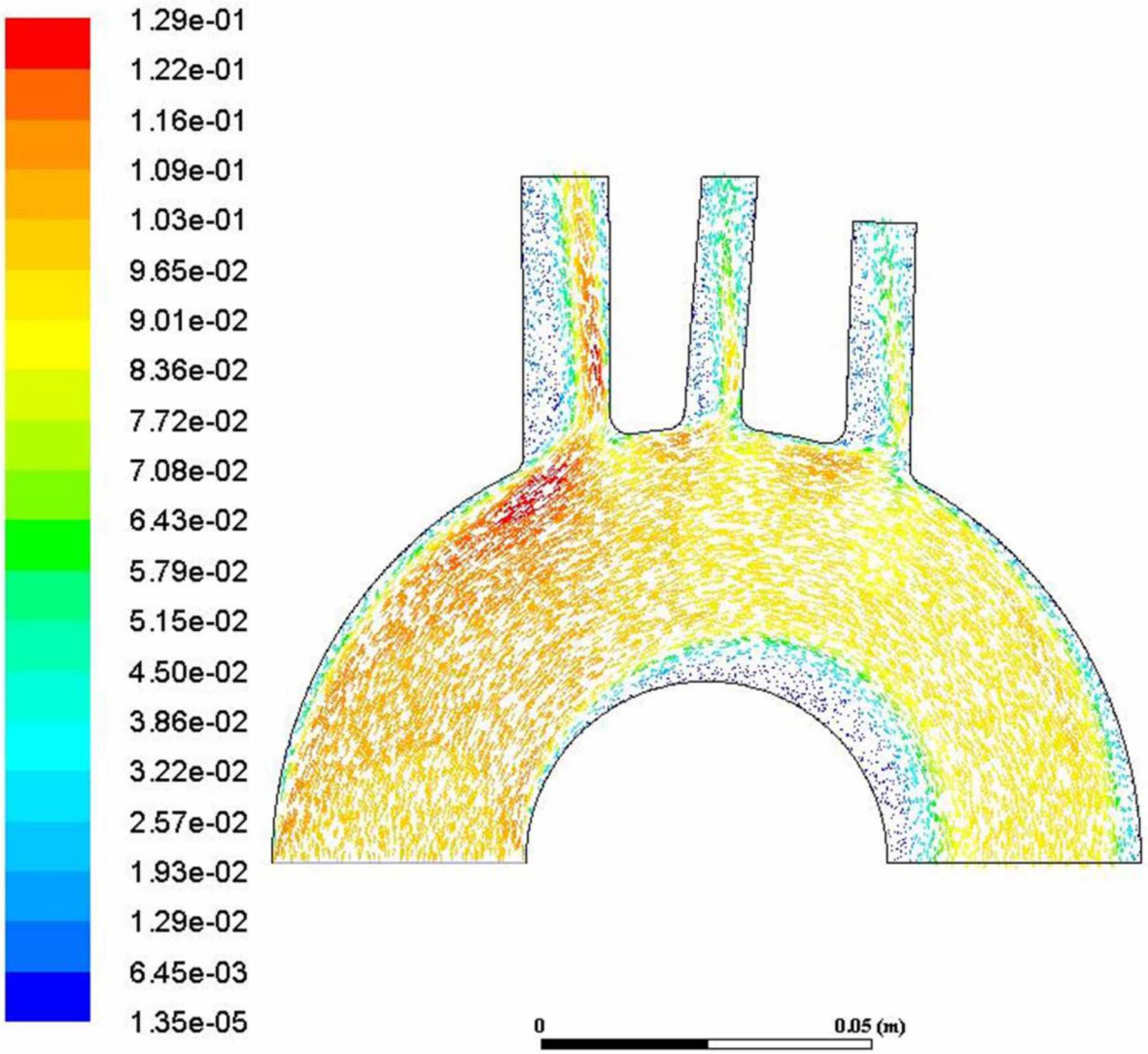

Figure 23:Velocity vector field at 30 degrees Celsius

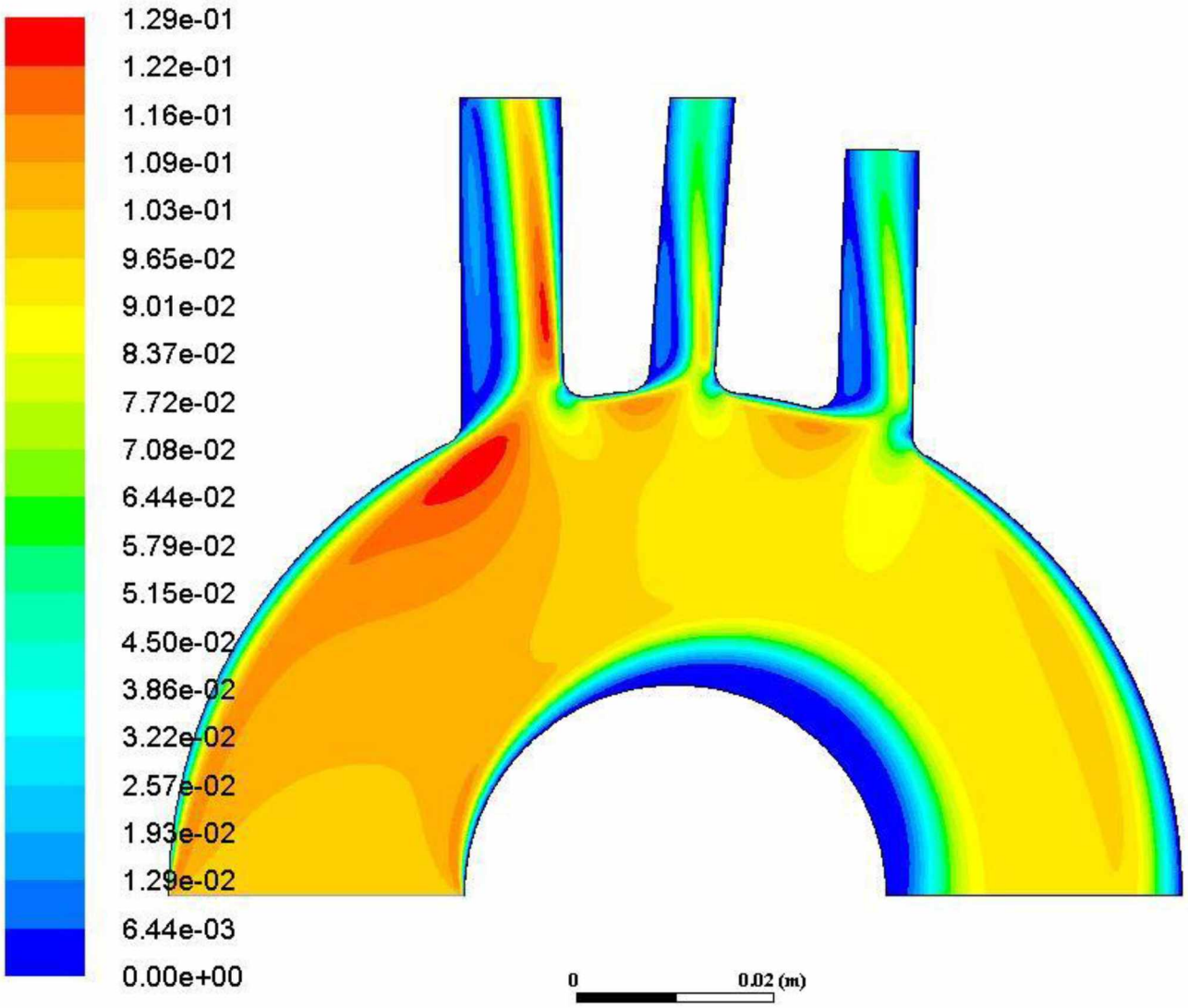

Figure 24:Velocity contour at 31 degrees Celsius

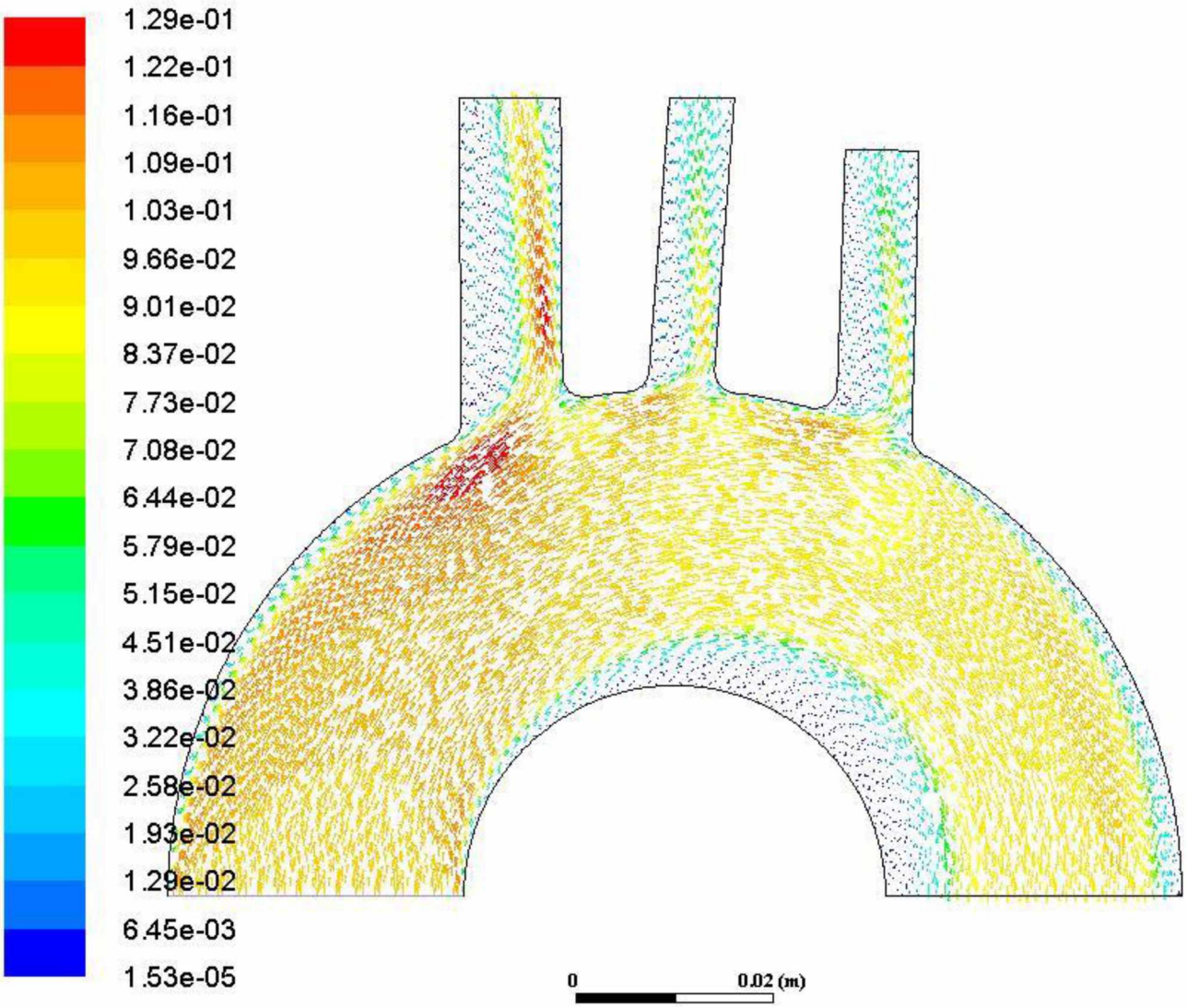

Figure 25:Velocity vector field at 31 degrees Celsius

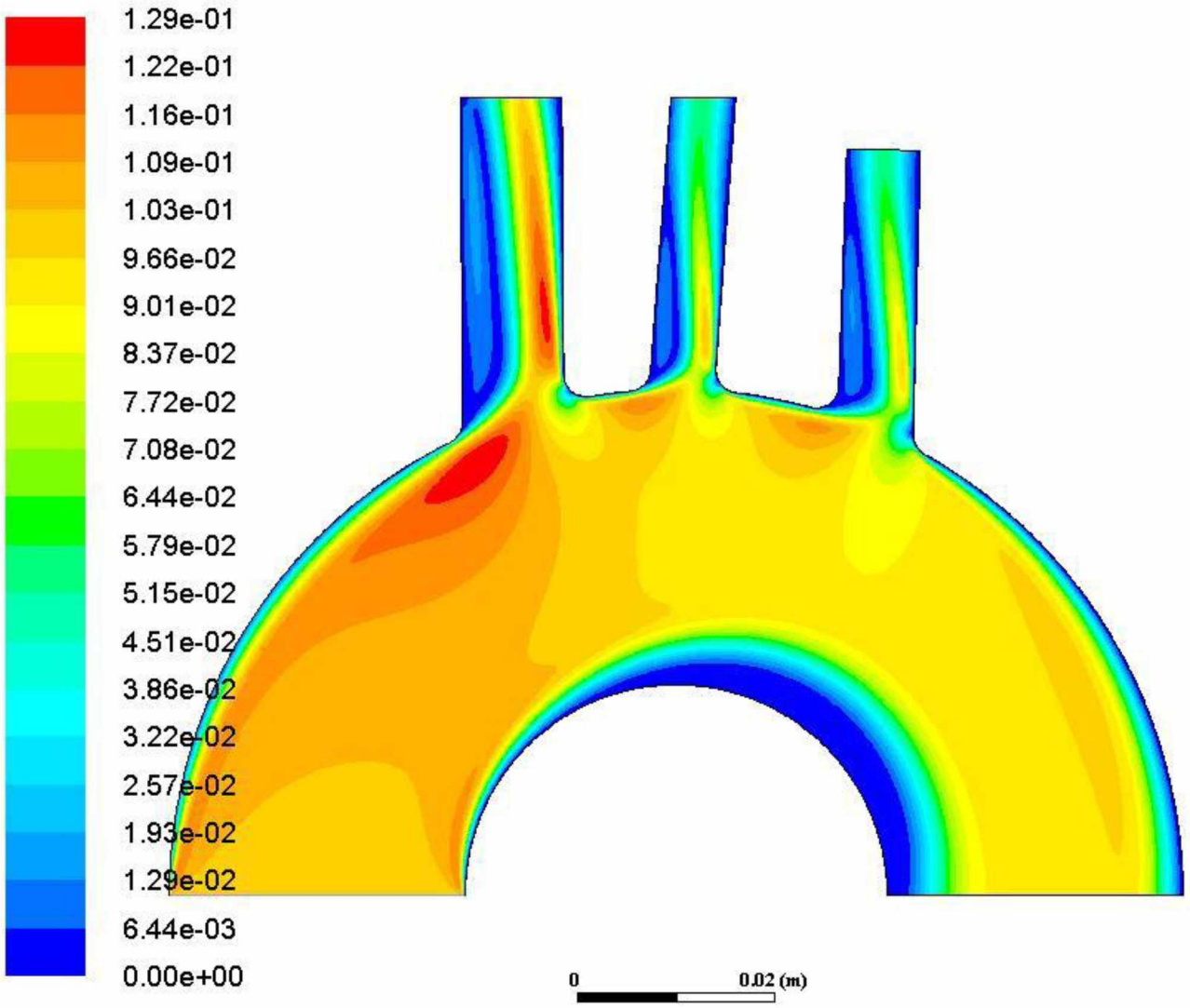

Figure 26:Velocity contour at 32 degrees Celsius

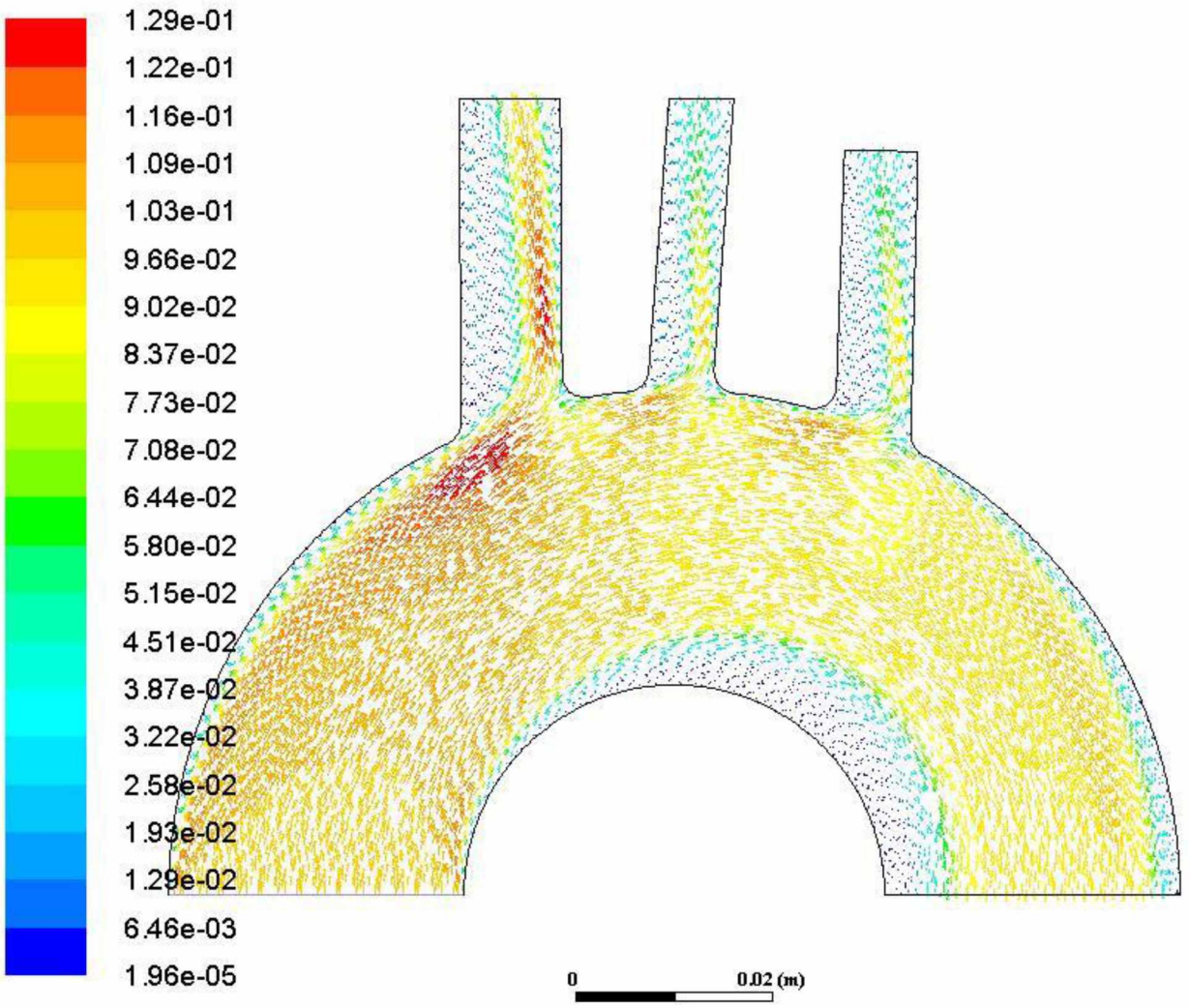

Figure 27:Velocity vector field at 32 degrees Celsius

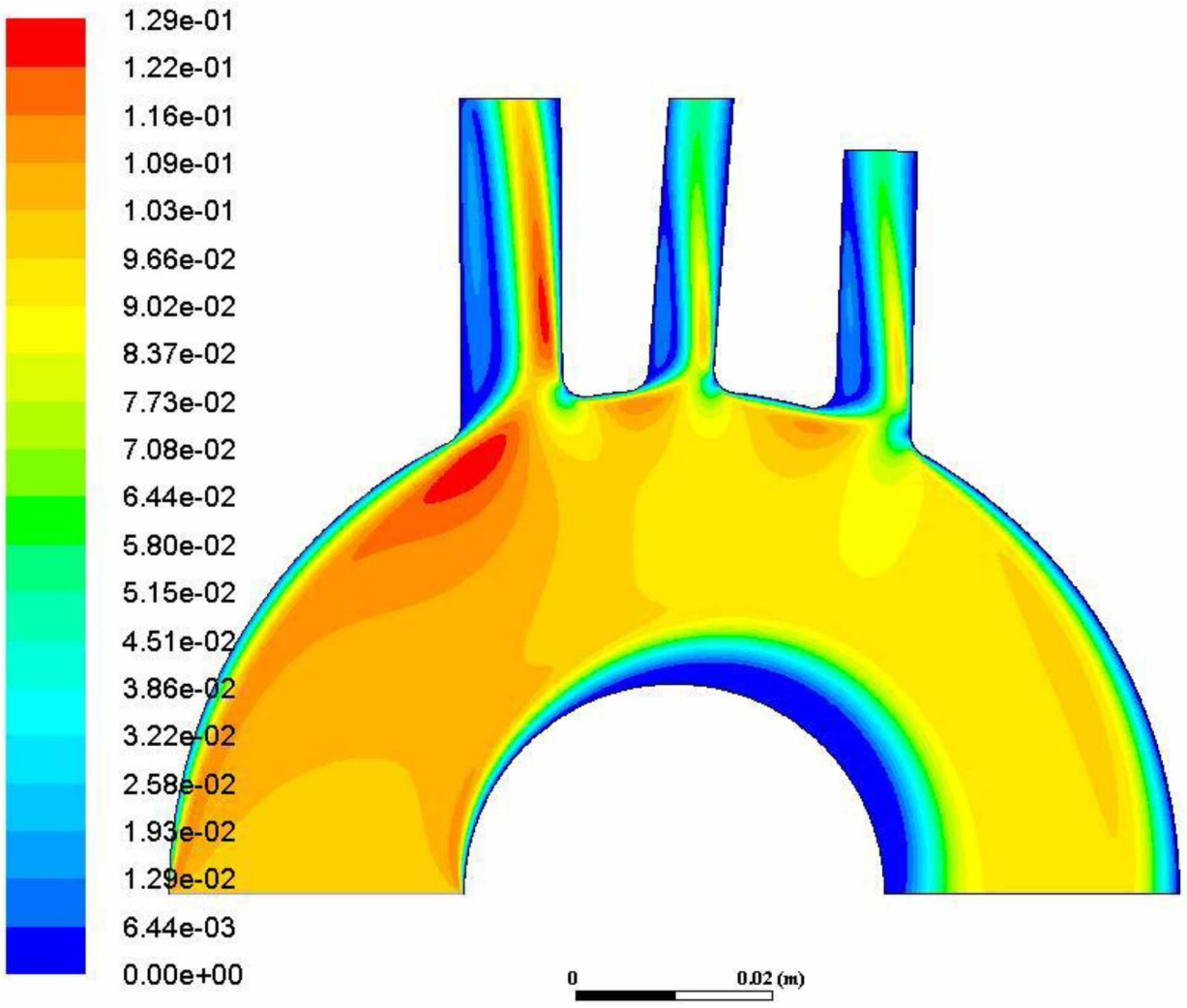

Figure 28:Velocity contour at 33 degrees Celsius

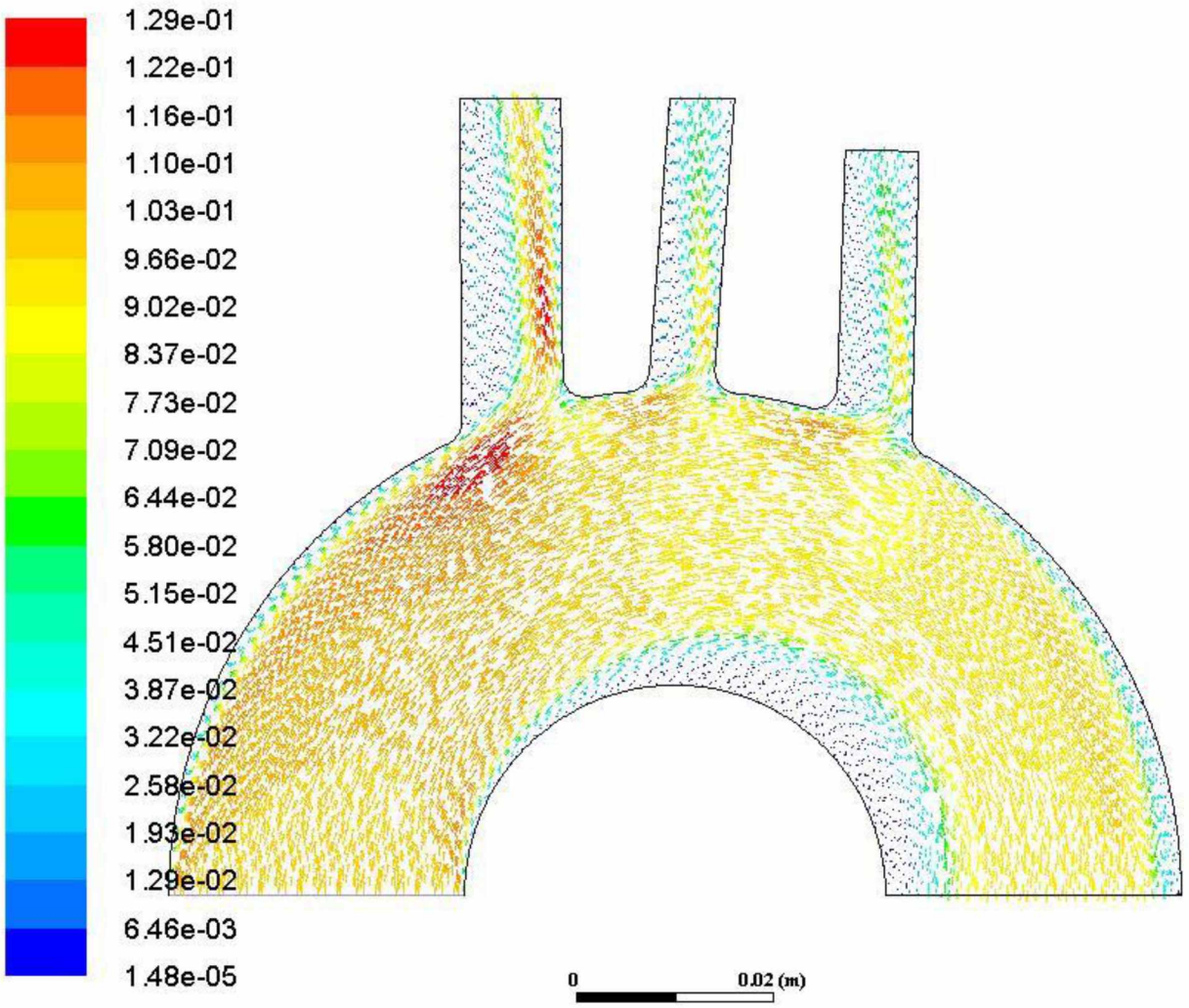

Figure 29:Velocity vector field at 33 degrees Celsius

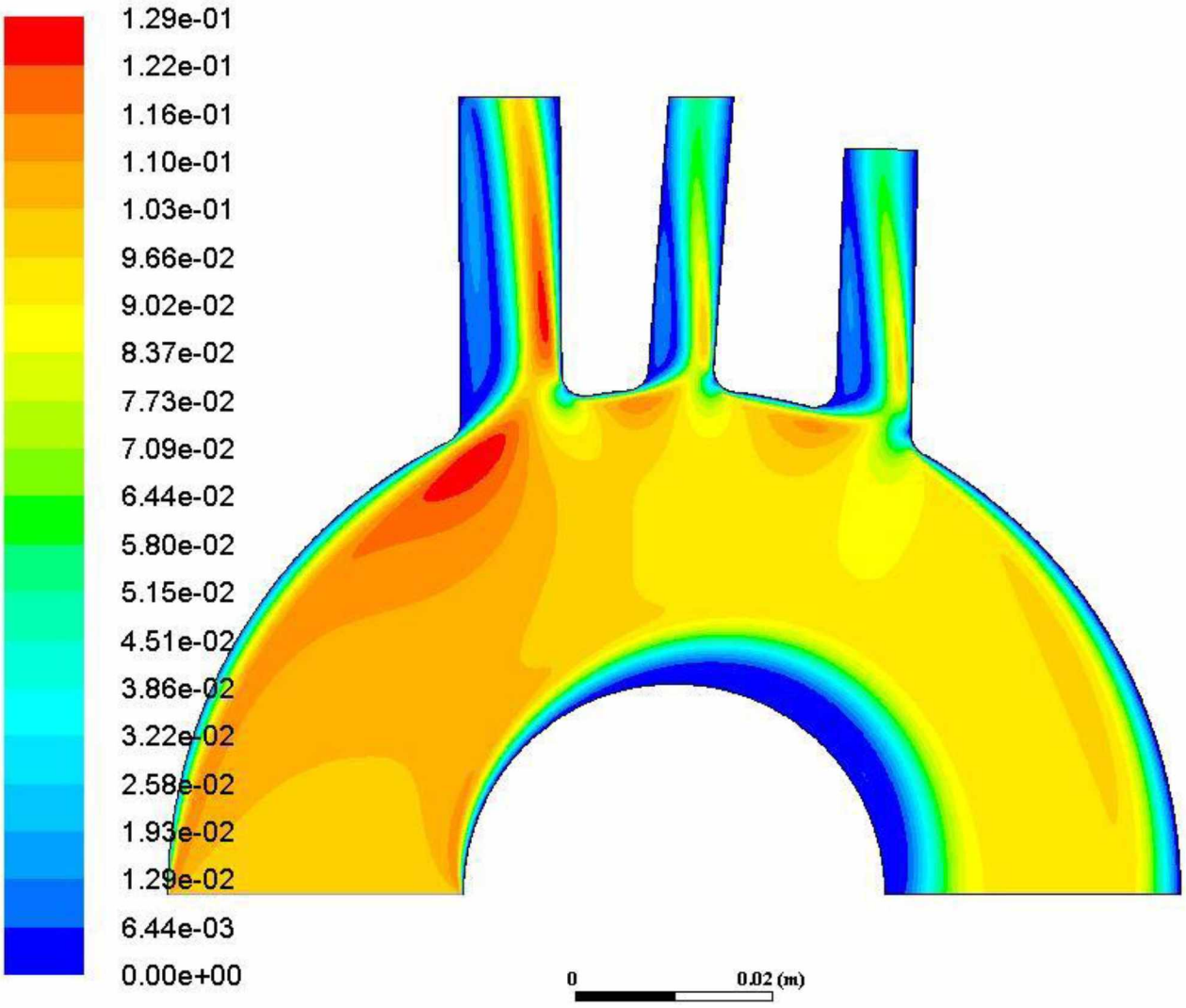

Figure 30:Velocity contour at 34 degrees Celsius

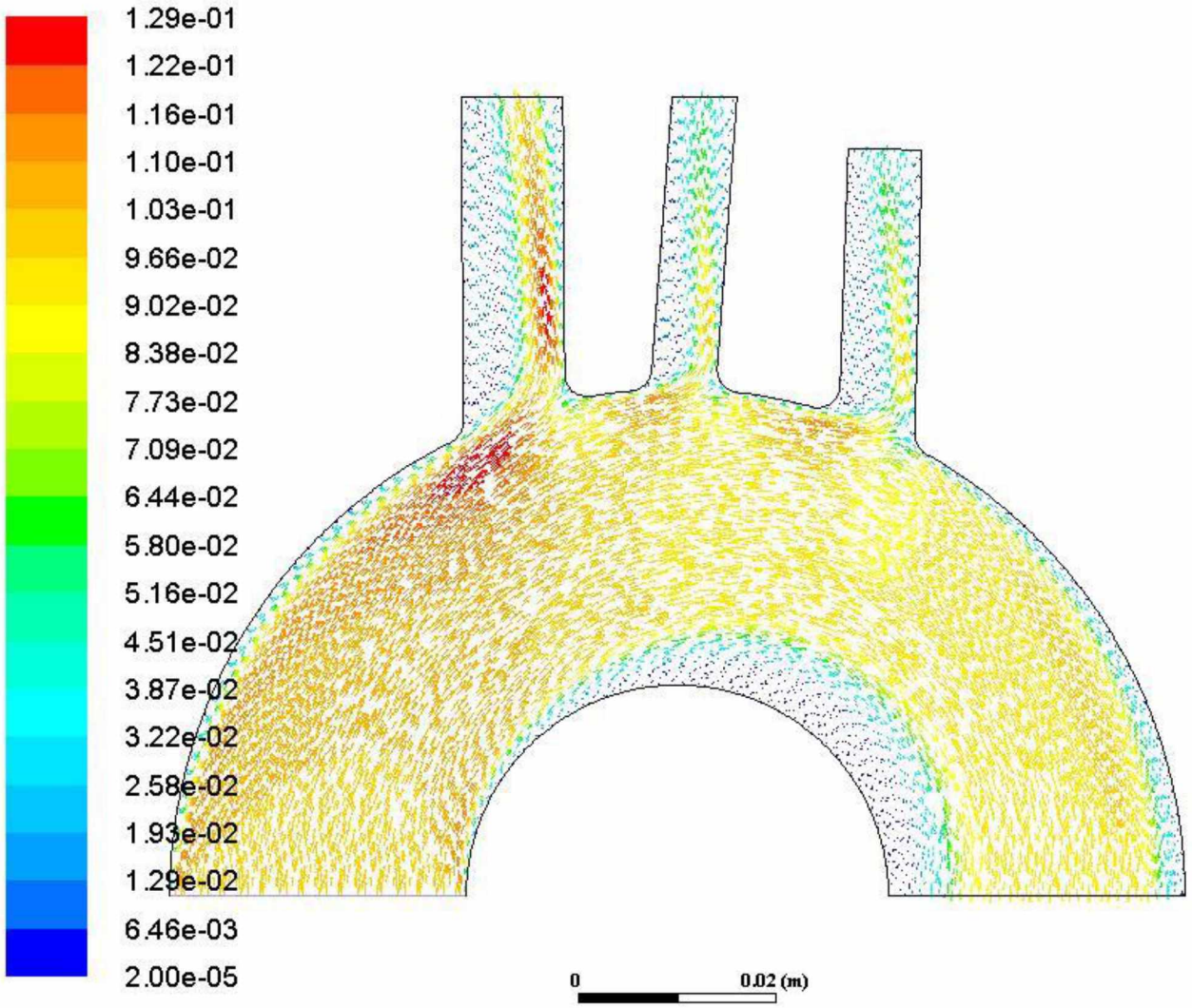

Figure 31:Velocity vector field at 34 degrees Celsius

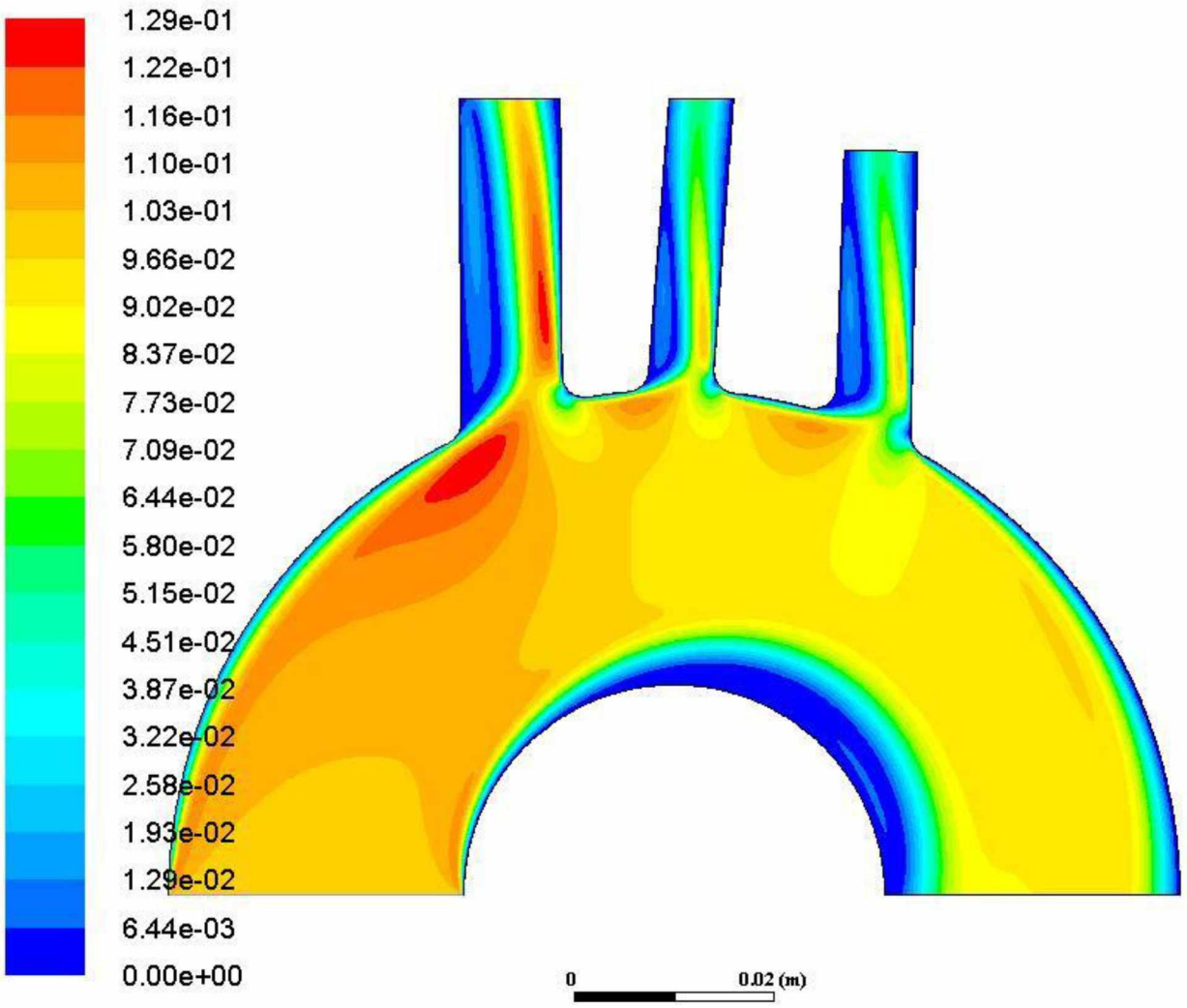

Figure 32:Velocity contour at 35 degrees Celsius

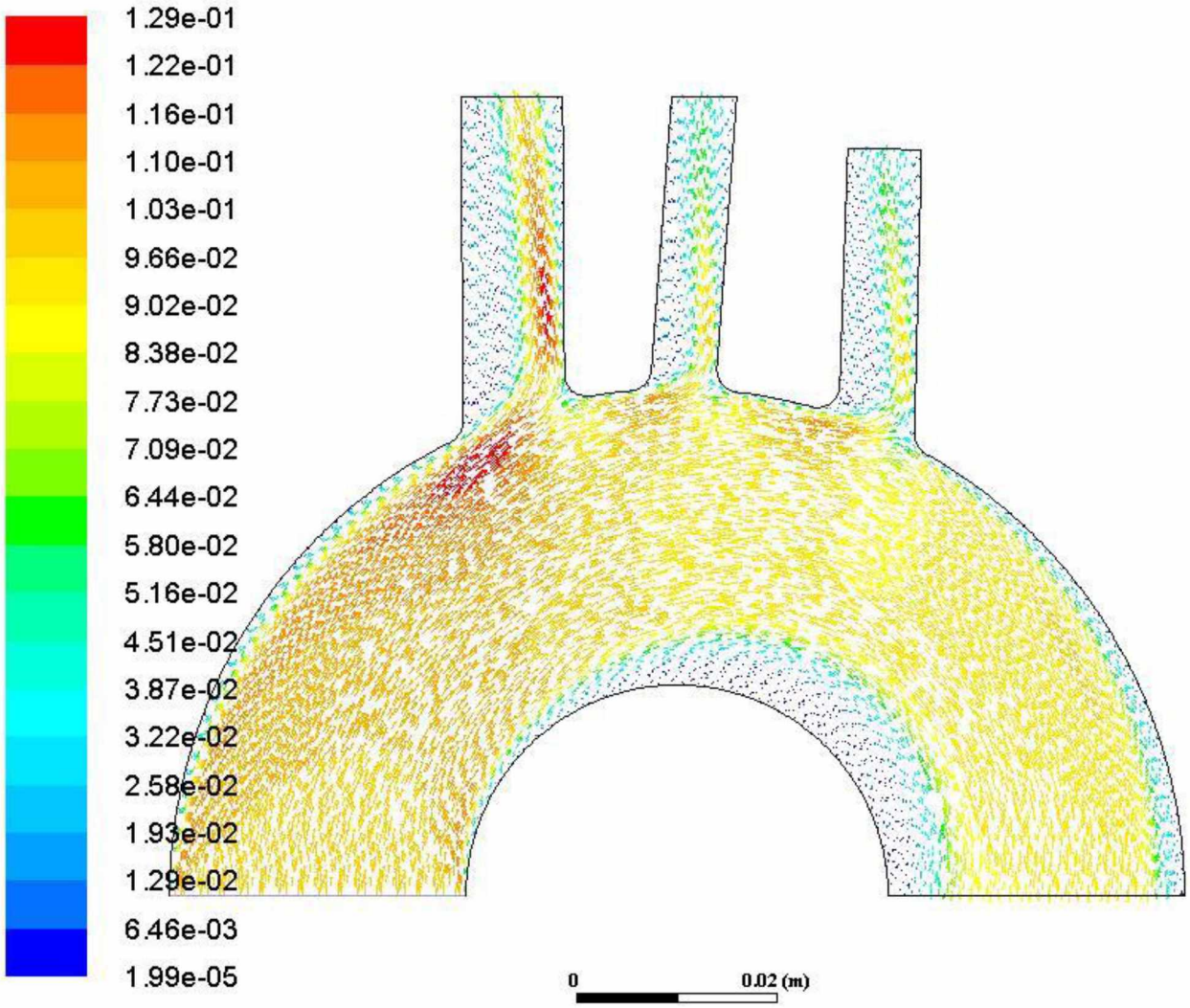

Figure 33:Velocity vector field at 35 degrees Celsius

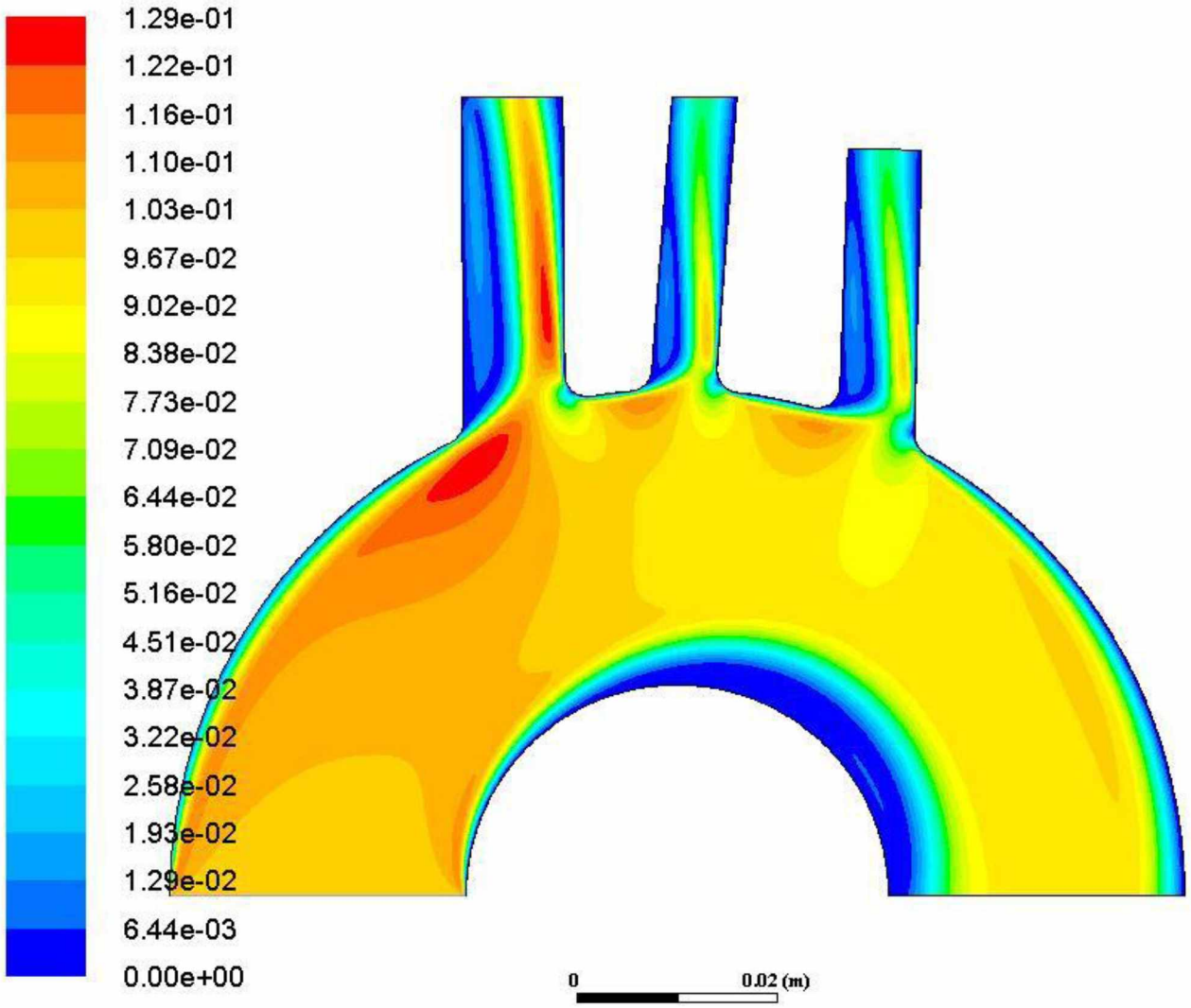

Figure 34:Velocity contour at 36 degrees Celsius

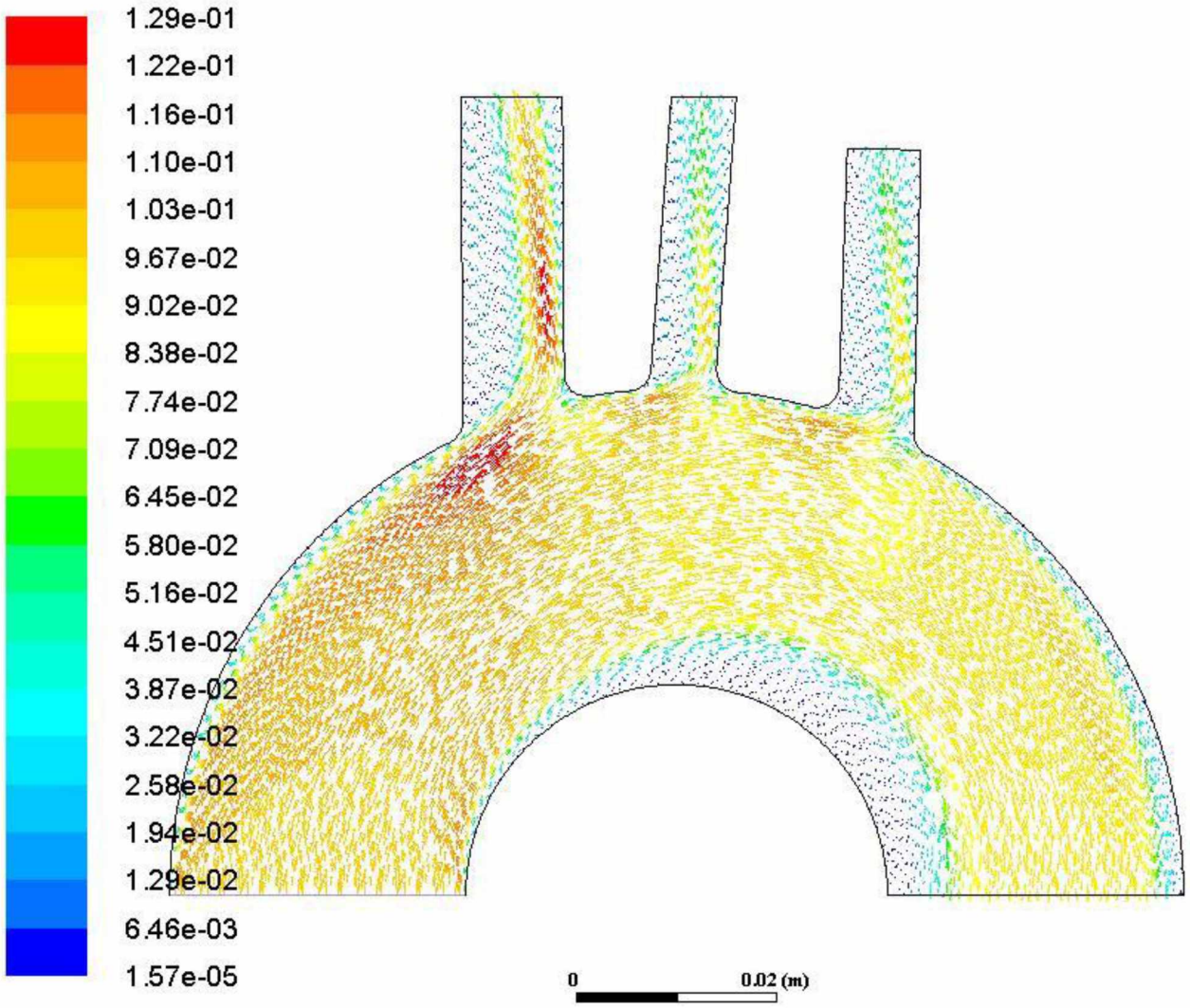

Figure 35:Velocity vector field at 36 degrees Celsius

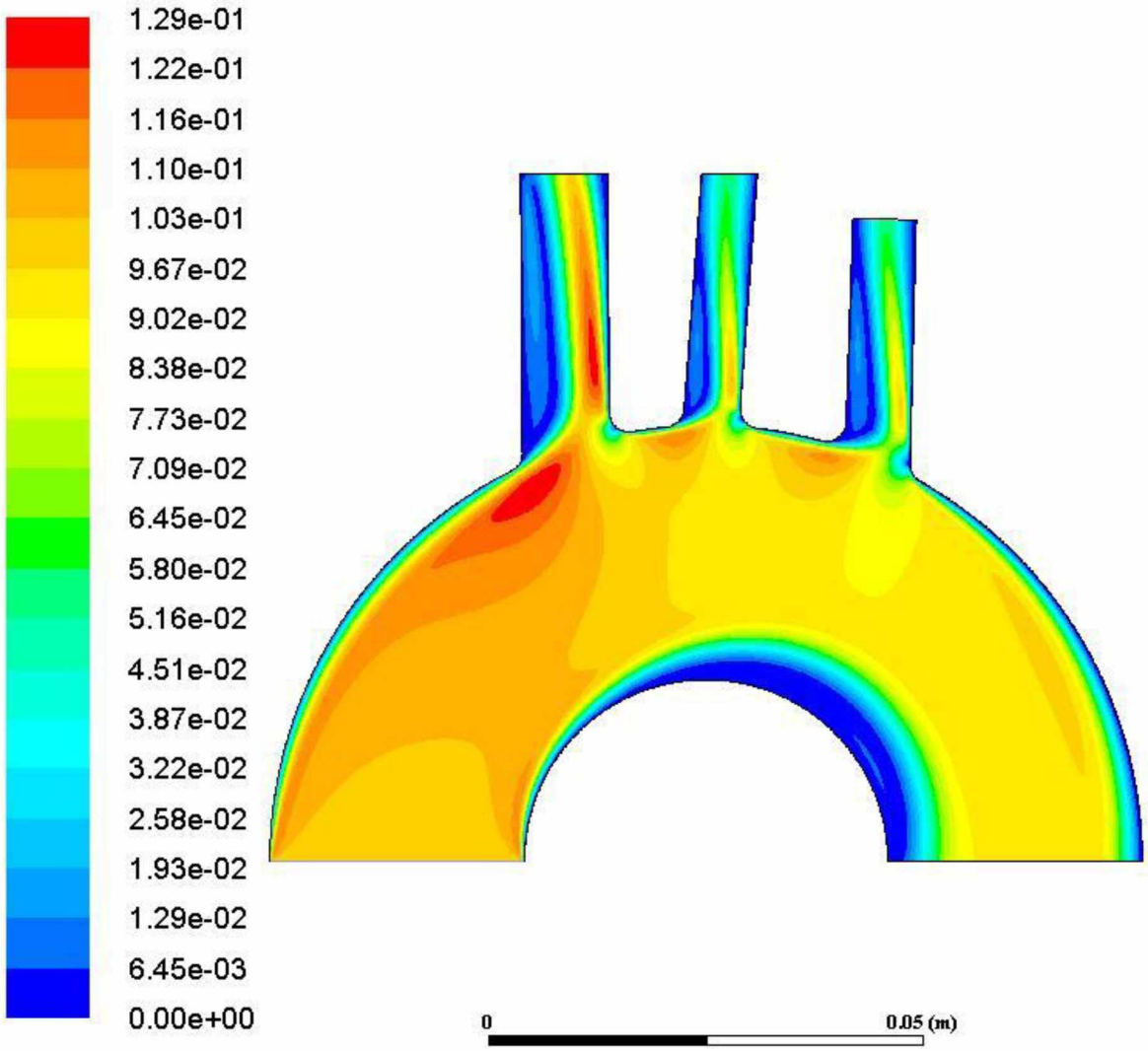

Figure 36:Velocity contour at 37 degrees Celsius

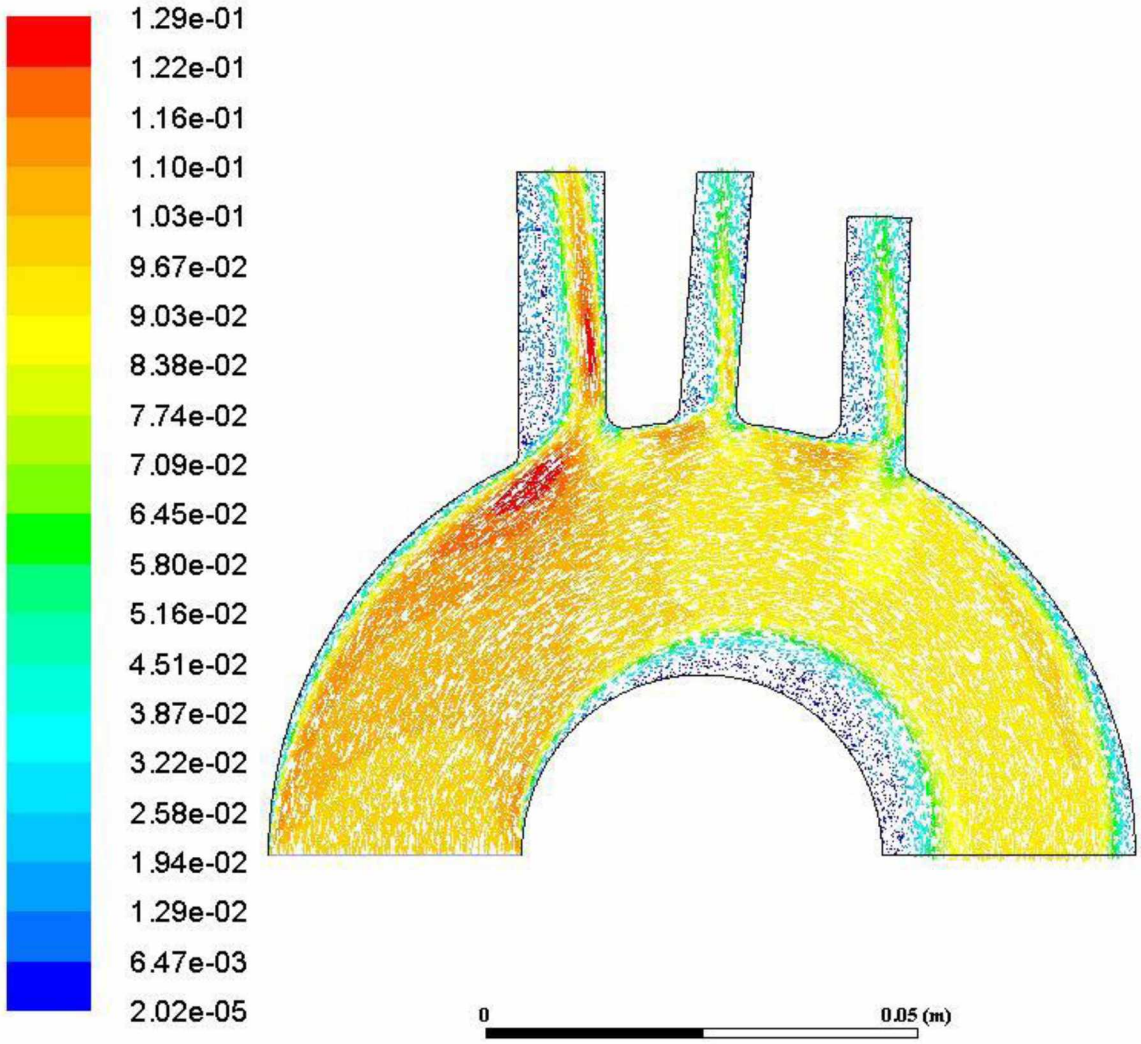

Figure 37:Velocity vector field at 37 degrees Celsius

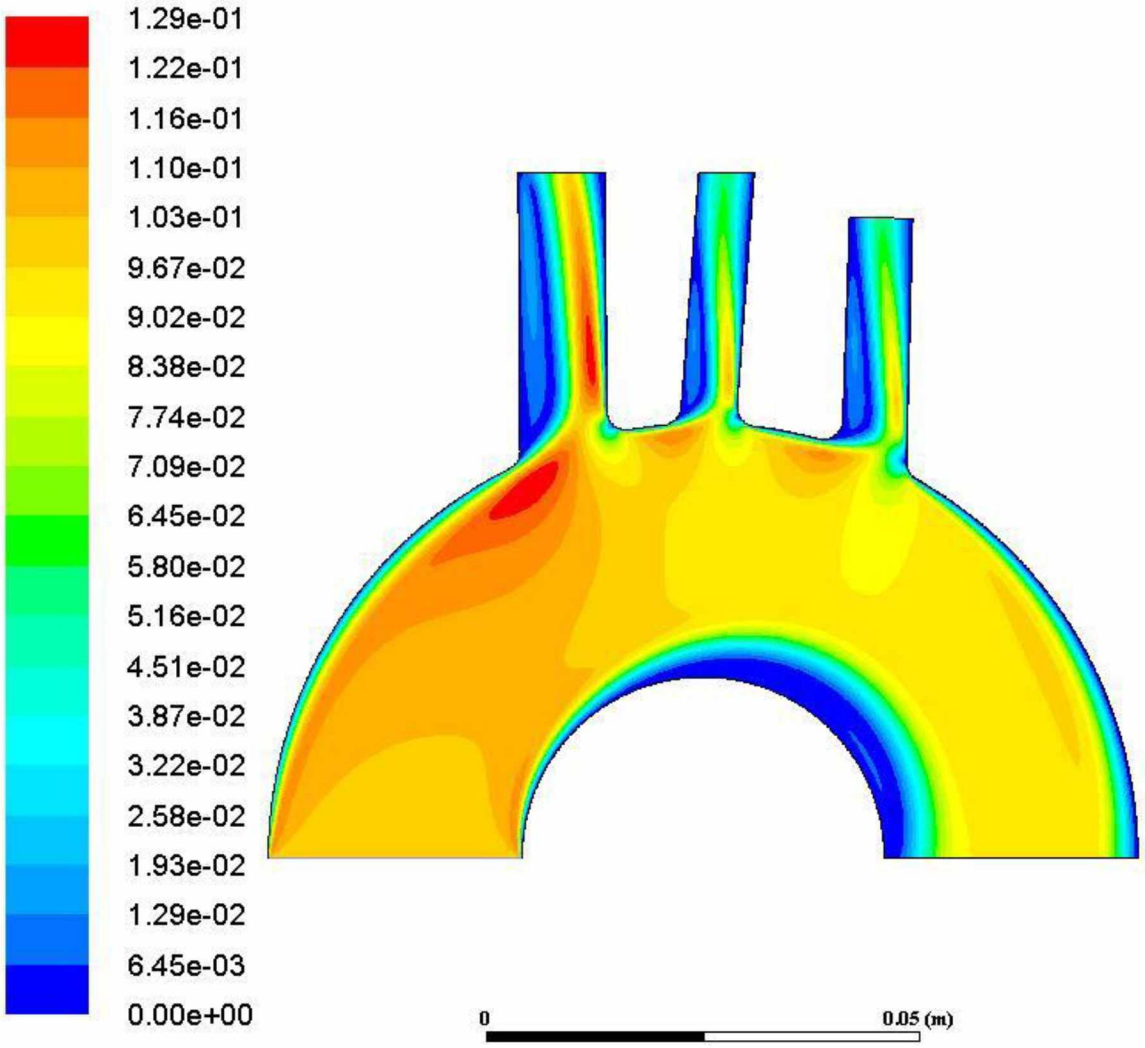

Figure 38:Velocity contour at 38 degrees Celsius

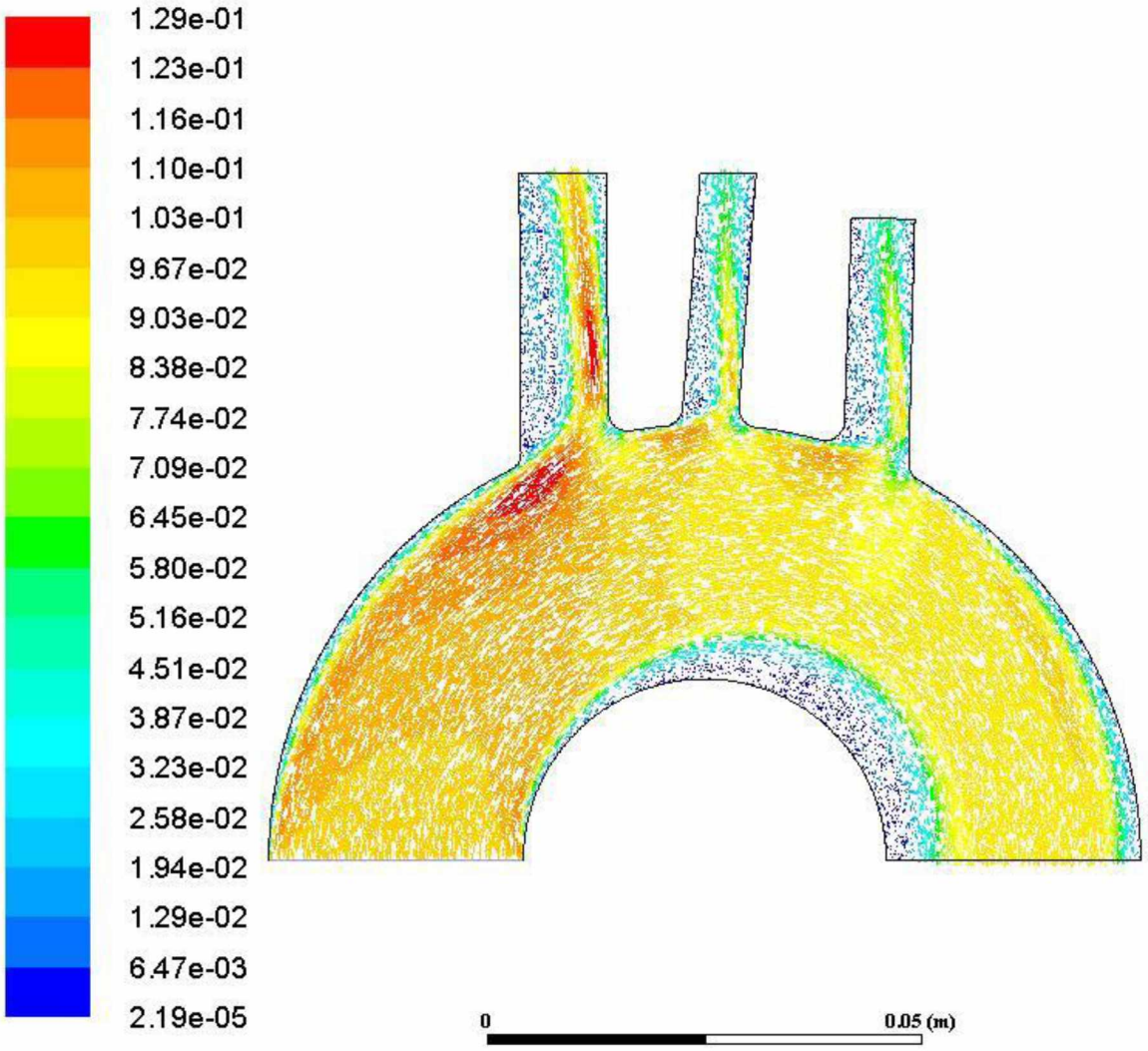

Figure 39:Velocity vector field at 38 degrees Celsius

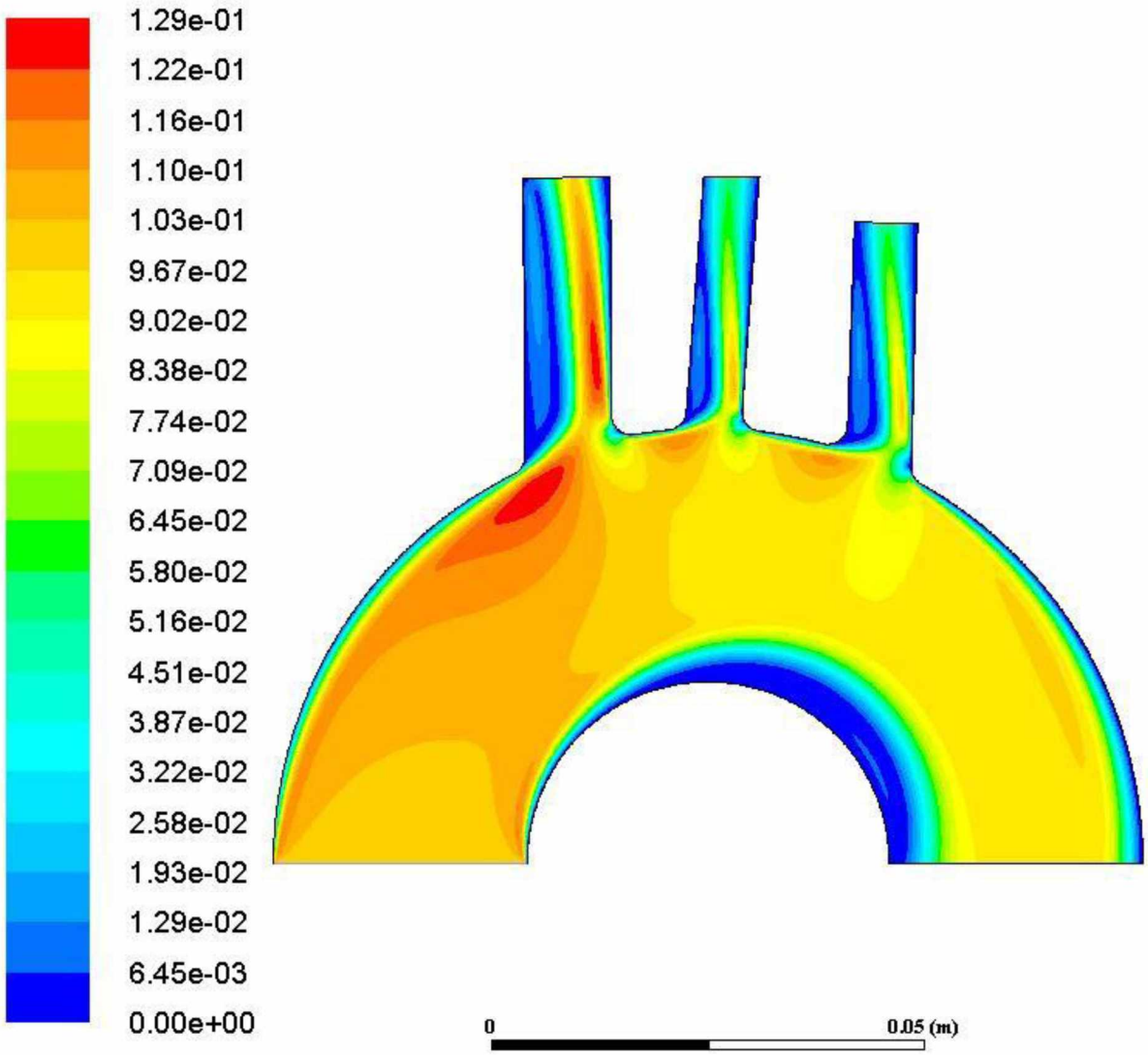

Figure 40:Velocity contour at 39 degrees Celsius

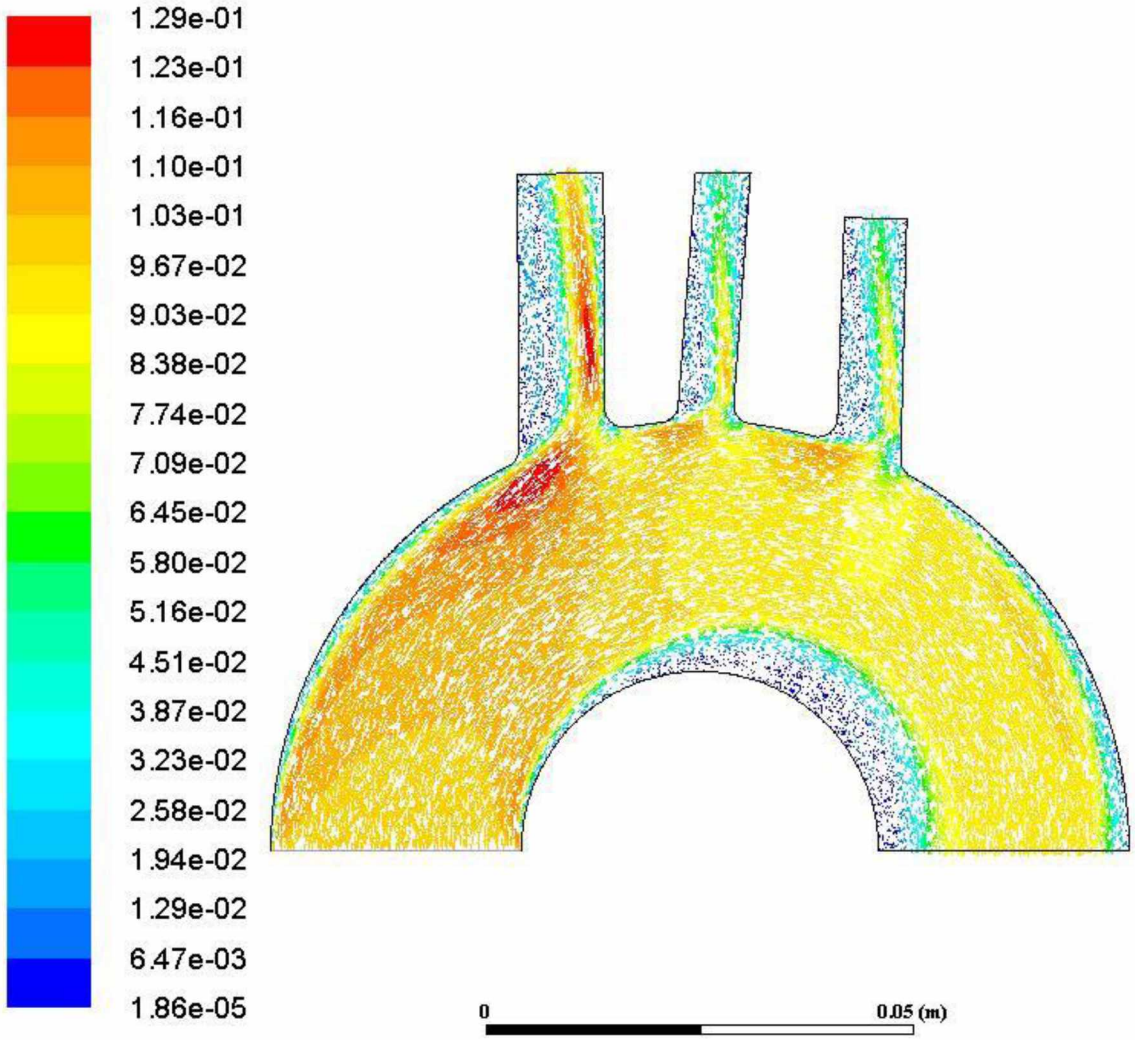

Figure 41:Velocity vector field at 39 degrees Celsius

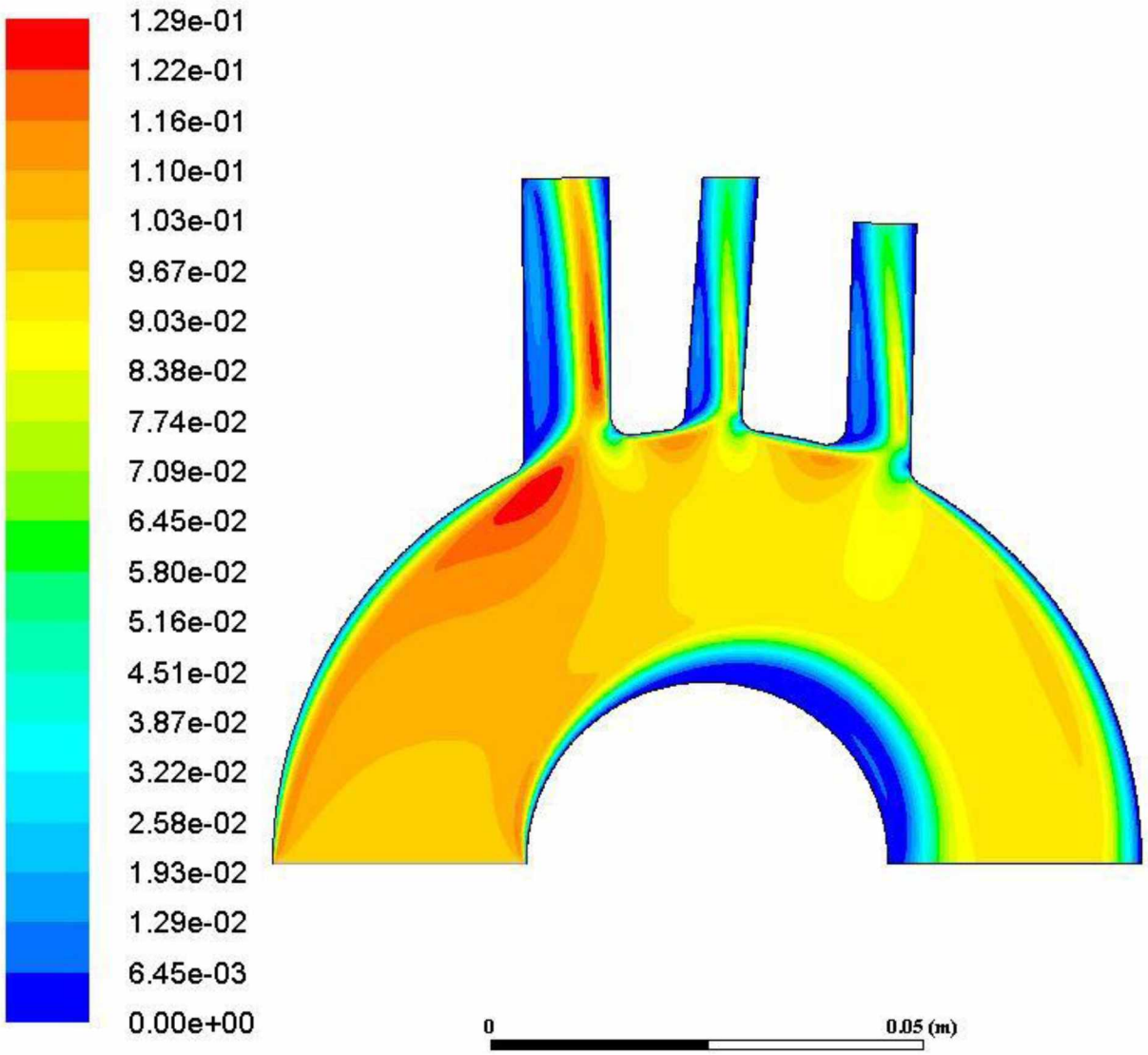

Figure 42:Velocity contour at 40 degrees Celsius

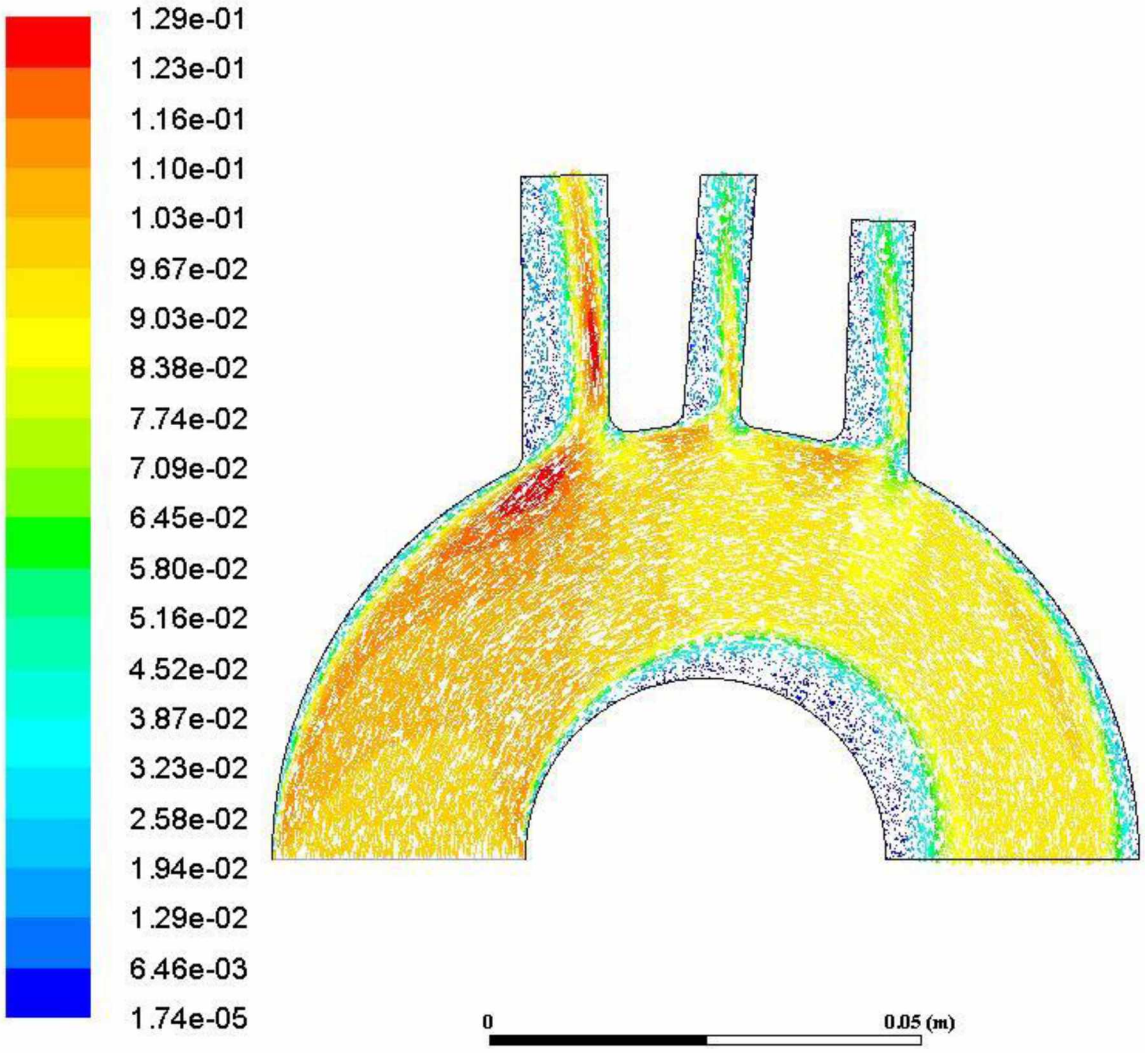

Figure 43:Velocity vector field at 40 degrees Celsius